Acta Geodyn. Geomater., Vol. 21, No. 4 (216), 309–328, 2024
DOI: 10.13168/AGG.2024.0026
journal homepage: https://www.irsm.cas.cz/acta

ORIGINAL PAPER

SHEAR STRESS-STRAIN RELATIONSHIPS AND ANISOTROPY IN SILTY SOIL: THE ROLE OF PRINCIPAL STRESS ROTATION

Farhad JAMIL [1], Changnv ZENG [1]*, Yuan MA [2], Soe Hlaing TUN [1] and Sharafat ALI [1]

[1] *School of Civil Engineering and Architecture, Henan University of Technology, Zhengzhou 450001, China*
[2] *China Shanxi Sijian Group CO., LTD, Xiaodian District, Taiyuan, 030012, China*

**Corresponding author's e-mail:* zengcnv@126.com

ARTICLE INFO

Article history:
Received 2 September 2024
Accepted 23 October 2024
Available online 7 November 2024

Keywords:
Hollow Cylindrical Apparatus
Principal Stress Rotation
Silt Soil
Stress Path
Intermediate Principal Stress

ABSTRACT

This study uses a hollow cylindrical apparatus to explore the effects of principal stress rotation on saturated silty soil, focusing on the static characteristics affected by cycle counts, intermediate principal stress coefficient (*b*), and rotational angle (α). As the principal stress axis rotates, strain fluctuations decrease and stabilize, with consistent strain trends observed across various *b* values. Anisotropy appears around 60° during the first cycle, significantly impacting radial strain while torsional shear strain remains less affected. Distinct hysteresis loops in shear stress-strain relationships reveal initial unclosed forms due to plastic strain accumulation, transitioning to closed loops with increased cycling, and showing noticeable variations in shear stiffness. As *b* values rise, stiffness degrades, influenced by both *b* values and *a* angles. Volumetric strain shows a linear increase for two cycles before decelerating, with *b*=1 demonstrating anisotropy at 60° and other values at 90°. Minimal contraction occurs for *b*=0 after the tenth cycle, while *b*=0.5 sees significant volume reduction. Higher *b* values also reduce non-coaxial behavior, linked to the initial principal stress orientation. These findings enhance the understanding of silty soil behavior under stress rotation, offering valuable insights for geotechnical engineering applications.

LIST OF ABBREVIATION AND NOTIONS

Hollow cylindrical apparatus (HCA),
Cyclic stress rotation (CSR),
Principal stress rotation (PSR),
Dynamic Triaxial Test System (DYNTTS),
Dynamic Hollow Cylinder Torsional Shear Test System (DYNHCA),
Intermediate principal stress coefficient (*b*),
Principal stress rotation angle (*a*),
Axial force (W),
Torque (T),
Outer radius (r_o),
Inner radius (r_i),
Outer confining pressure (P_o),
Inner confining pressure (P_i),
Axial stress (σz),
Radial stress (σr),
Circumferential stress (σθ),
Torsional shear stress (τzθ),
Initial consolidation inclination angle ($\zeta^{\circ\circ}$),
Axial strain (ε_z),
Radial strain (ε_r),
Circumferential strain (ε_θ),
Torsional shear strain ($\gamma_{z\theta}$),
Degree of non-coaxiality (β),
Principal strain increment direction (βdε).

1. INTRODUCTION

Silt deposits consist of a combination of sand, silt, and clay particles that are extensively distributed throughout the regions of the Yellow River and extend into the marine areas of the Bohai Sea. These types of soils are typically inadequately graded and have long been deemed unsuitable for construction purposes. However, due to the ongoing economic development in the region, various construction projects on silty sand have been undertaken, including activities such as excavation and pit filling, embankment construction, and underground engineering. These construction endeavors often involve principal stress rotation characterized by fluctuations in both the magnitude and direction of the primary stresses. As a result, challenges pertaining to strength and deformation failures arise (Gao and Zhao, 2017; Lade and Kirkgard, 2000; Qian et al., 2018; Wang et al., 2019). In primary stress rotation, silty soil demonstrates dynamic responses, including changes in strain patterns and non-coaxial behaviour, which are less evident in static or unidirectional stress situations. In static conditions, the soil's behaviour is more consistent and predictable, mainly influenced by its consolidation and shear strength. In contrast, stress rotation can induce varying levels of anisotropy, leading to altered failure mechanisms and an increased risk of shear formation. This results in heightened sensitivity to loading direction and a more intricate

Cite this article as: Jamil F, Zeng C, Ma Y, Ali S, Tun S H: Shear stress-strain relationships and anisotropy in silty soil: The role of principal stress rotation. Acta Geodyn. Geomater., 21, No. 4 (216), 309–328, 2024. DOI: 10.13168/AGG.2024.0026

relationship between stress and strain, producing unique mechanical behaviours that differ from those observed in static conditions.

Therefore, it is essential to look at the effects of the principal stress rotation angle and intermediate principal stress coefficient when examining the mechanical behavior of silty sand in the Yellow River zone. Such an investigation is crucial in order to provide reliable guidance for these infrastructure projects. In the current study, we comprehensively address silty soil deformation behavior and its anisotropic characteristics. More specifically, the study aimed to investigate the connections between shear stress, the pattern of strain development, and alterations in volume.

The rotation of principal stresses is inherent in numerous geotechnical scenarios, especially when soil experiences non-coaxial loading conditions. When the major primary stress rotation and the intermediate principal stress coefficient are taken into account, this behavior becomes even more apparent. These dynamic factors greatly influence the strain patterns in silty soils, thus making it essential to comprehensively investigate the implications of principal stress rotation on their mechanical behavior. Research into the unique stress paths experienced by soil dynamics commences by investigating the principal stress axis rotation. (Dareeju et al., 2017; Gallage et al., 2016; Inam et al., 2012) Conducted tests to replicate the rotation of the primary stress axis caused by traffic loads, confirming that different subgrade materials experience gradual cyclic plastic deformation as a significant consequence of this rotation. Qian et al. (2018) conducted a study to investigate how traffic loads affect the stress-strain response of completely saturated soft clay, with a specific emphasis on the influence of the rotation of principal stresses. A comparative examination was conducted by Wang et al. (2017) in order to assess the cyclic endurance of sand on the seabed by means of the impact of both a circular stress trajectory and an unconventional elliptical stress trajectory.

Silty soil is known for its anisotropic behavior; non-uniform strain patterns with varying magnitudes and orientations of strains throughout the soil mass result from inclined consolidation. In certain engineering scenarios, such as the construction of slopes, the preparation of subgrade, and the excavation of extensive foundation pits, it is possible for the principal stress axis of the soil to deviate from its perpendicular alignment with the horizontal direction during the process of consolidation. Jardine et al. (1986) in the context of multistage embankment projects, it is crucial to account for the consolidation of soil elements. In the course of inclined consolidation, the major principal stress will show distinctive orientations for soil elements located at different depths below the central line of the embankment, as depicted in Figure 1.

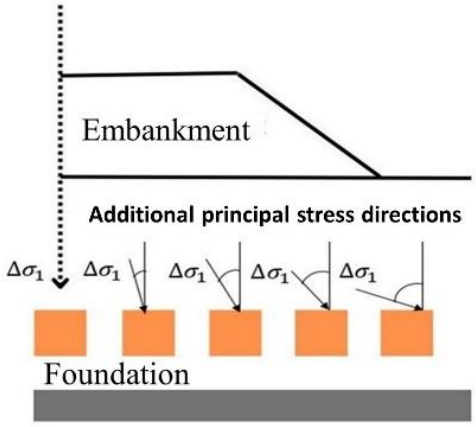

Fig. 1 Soil element in stress under an embankment.

Until the present a considerable amount of laboratory experiments were performed without drainage and focused on evaluating the soil potency, its alteration conduct, and the formation of pore-water pressure in the absence of drainage (Ishihara and Towhata, 1983; Nakata et al., 1998; Yang et al., 2007). These examinations were performed on soils experiencing cyclic rotation of the principal stress axes, as this rotation is fundamental for understanding soil deformation behavior. Contrasting the outcomes obtained from experiments carried out under drained and undrained circumstances demonstrates that in drained experiments the paths of effective stress can be deliberately regulated. The execution of drained experiments allows for a more precise determination of the stress-strain relationship and the mechanism of deformation. Concurrently, volumetric deformation that occurs in studies where excess pore water is removed does indeed provide a direct sign of the possibility of pore water pressure forming. (Shamoto et al., 1998a, 1998b; Wong and Arthur, 1986). The rotational movement of the primary stress possesses the capacity to yield the build-up of an excessive volume of pore water pressure and plastic deformation. These factors, when present in undrained conditions, have the capability to expedite the process of liquefaction (Wang et al., 2022). The cumulative generalized shear strain in marine silt that is saturated and exposed to principal stress rotation due to wave loading is significantly affected by both the cyclic stress ratio (CSR) and the amplitude ratio of cyclic loading, which is represented as δ. An increase in the CSR leads to an increase in the cumulative generalized shear strain, whereas an increase in δ results in a decrease in the cumulative generalized shear strain (Cui et al., 2021). The utilization of PSR in geotechnical experiments has the capability to produce supplementary excess pore water pressures and plastic strains, which subsequently expedites the process of liquefaction in conditions where drainage is absent.

The conventional triaxial test is extensively employed to assess the mechanical properties of soils.

However, a significant limitation of this test is its ability to apply only either compressive or tensile stress to a soil element. Conversely, in order to acquire a thorough and all-encompassing outlook on the behavior of soil that lacks cohesion, it is absolutely crucial to possess knowledge and comprehension of its response when subjected to stress conditions that are generalized in nature. The hollow-cylinder apparatus (HCA) is capable of facilitating complex stress paths that entail alterations to the principal stress directions (Hight et al., 1983; Kumruzzaman and Yin, 2012; Miura et al., 1986; Wang et al., 2017). An extensive and continuous examination has been carried out to investigate the properties of silt, sand, and clay through the utilization of the HCA. These inquiries have predominantly concentrated on stress paths that encompass alterations in the major principal stress orientation denoted as *a* and the intermediate principal stress coefficient known as *b* (Hight et al., 1983; Nakata et al., 1998; Symes et al., 1988, 1984; Yang et al., 2007; Yoshimine et al., 1998). The parameter *a* signifies the magnitude of the angle defined by between the primary principal stress's direction and the vertical axis. $a = \frac{1}{2}\, arctan\, \frac{2\tau}{\sigma z - \sigma\theta}$ while, the coefficient of intermediate principal stress defined as $b = \frac{\sigma 2 - \sigma 3}{\sigma 1 - \sigma 3}$

Existing literature offers limited insights about the principal stress rotation influence on silt soil behavior. (Zhang et al., 2019; Zhou et al., 2018) Employed a cylindrical torsion shear apparatus with a hollow structure to conduct experiments on saturated silt. These experiments included different ratios of cyclic loading amplitudes in both axial and torsional modes and also involved simulations of dynamic stress paths that were either circular or elliptical. These investigations revealed the substantial impact of dynamic stress paths on the liquefaction tendencies of saturated silt. Silty soils present unique challenges in foundation and embankment engineering due to their intermediate characteristics between sand and clay. They are typically known for their low shear strength, high compressibility, and high sensitivity to changes in moisture content, making them difficult to manage in geotechnical applications. A key gap in existing research lies in the limited understanding of how silty soils respond to complex stress paths and principal stress rotations conditions often encountered in real-world geotechnical environments.

This study addresses this gap by focusing on the behavior of silty soils under principal stress rotation using a hollow cylindrical apparatus. Specifically, it investigates the influence of cycle count on the static characteristics of saturated silty soils, with an emphasis on the intermediate principal stress coefficient *b* and the rotational angle α. The research provides a comprehensive analysis of the anisotropic properties of saturated silt soil under drained conditions, considering factors such as stress relationships, deformation patterns, volumetric changes, and strength characteristics. The significance of this study is particularly important for region like the Yellow River basin, where silty soils are prevalent, and infrastructure development is ongoing. By understanding how principal stress rotation affects silty soils, this research offers valuable insights that enhance the understanding of subgrade soil stress states in practical engineering applications. The results will contribute to developing more accurate design guidelines for road construction, foundation stability, and infrastructure projects, ultimately supporting safer and more efficient geotechnical solutions in regions with significant silt deposits.

The remainder of this paper is organized as follows: Section 2 presents the materials and methods used in the experimental setup, including detailed procedures for sample preparation and the testing process. Section 3 discusses the results, focusing on the strain behavior and stress response under varying *b* values during principal stress rotation. Provides a detailed analysis and interpretation of the findings, highlights the influence of the intermediate principal stress coefficient on shear stiffness and anisotropy. Section 4 discussed the validation of the study. Finally, section 5 concludes the study, offering insights into the practical implications of the results and suggesting directions for future research.

2. MATERIALS AND METHOD

The Hollow Cylinder Torsional Shear Apparatus (HCA), which has been designed by the UK-based company GDS, is utilized in the ongoing study. The HCA serves the purpose of attaining intricate stress paths and replicating the stress condition of soil in real road engineering circumstances. The HCA comprises two primary components: The Dynamic Triaxial Test System (DYNTTS) and the Dynamic Hollow Cylinder Torsional Shear Test System (DYNHCA). This system includes components such as an axial/torsional driving mechanism, a pressure chamber and controllers for internal and external confinement and back pressure, a stress and strain measurement setup, signal processing equipment, and a GDS digital control system. Figure 2, illustrates the hollow cylindrical torsion shear apparatus.

The application of the hollow cylindrical torsion shear apparatus involves the usage of a cylindrical sample that possesses a hollow interior. This sample is characterized by specific dimensions, which consist of a height denoted as H, measuring 200 mm. Additionally, the sample has an outer diameter referred to as ro, measuring 50 mm, and an inner diameter identified as ri, measuring 30 mm. The specimen is subjected to stress-strain components through the application of various factors such as internal confining pressure Pi, external pressure Po, axial force W and torque T. The DYNHCA generates four distinct stress constituents' namely axial stress σz, radial stress σr, circumferential stress σθ and torsional shear stress τzθ. In addition, it is capable of measuring the corresponding four strain components. Through the integration of these stress

Fig. 2 Hollow cylinder torsional shear apparatus.

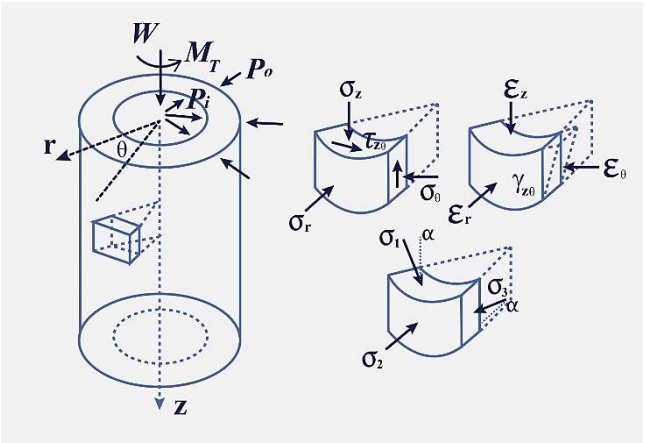

Fig. 3 Hollow cylindrical specimen in the stress state (Guo et al., 2021).

Table 1 Formulas used for the components of stress and strain (Hight et al., 1983).

Component	Stress	Strain
Axial	$\sigma_z = \frac{W}{\pi(r_o^2 - r_i^2)} + \frac{p_o r_o^2 - p_i r_i^2}{(r_o^2 - r_i^2)}$	$\varepsilon_z = \frac{z}{H}$
Radial	$\sigma_r = \frac{p_o r_o + p_i r_i}{r_o + r_i}$	$\varepsilon_r = -\frac{u_o - u_i}{r_o - r_i}$
Circumferential	$\sigma_\theta = \frac{p_o r_o - p_i r_i}{r_o - r_i}$	$\varepsilon_\theta = -\frac{u_o + u_i}{r_o + r_i}$
Shear	$\tau_{z\theta} = \frac{T}{2}\left(\frac{3}{2\pi(r_o^3 - r_i^3)} + \frac{4(r_o^3 - r_i^3)}{4\pi(r_o^2 - r_i^2)(r_o^4 - r_i^4)}\right)$	$\gamma_{z\theta} = \frac{2\theta(r_o^3 - r_i^3)}{3H(r_o^2 - r_i^2)}$
Major Principal	$\sigma_1 = \frac{\sigma_z + \sigma_\theta}{2} + \sqrt{\left(\frac{\sigma_z - \sigma_\theta}{2}\right)^2 + \tau_{z\theta}^2}$	$\varepsilon_1 = \frac{\varepsilon_z + \varepsilon_\theta}{2} + \sqrt{\left(\frac{\varepsilon_z - \varepsilon_\theta}{2}\right)^2 + \gamma_{z\theta}^2}$
Intermediate Principal	$\sigma_2 = \sigma_r$	$\varepsilon_2 = \varepsilon_r$
Minor Principal	$\sigma_3 = \frac{\sigma_z + \sigma_\theta}{2} - \sqrt{\left(\frac{\sigma_z - \sigma_\theta}{2}\right)^2 + \tau_{z\theta}^2}$	$\varepsilon_3 = \frac{\varepsilon_z + \varepsilon_\theta}{2} - \sqrt{\left(\frac{\varepsilon_z - \varepsilon_\theta}{2}\right)^2 + \gamma_{z\theta}^2}$

and strain elements, the hollow cylindrical torsion shear apparatus can achieve intricate and continuous stress path rotations. The stress-strain condition of the hollow cylindrical sample throughout the testing procedure is depicted in Figure 3. Table 1 contains the formulas for calculating the stress and strain components (Hight et al., 1983).

2.1. SAMPLE PREPARATION AND TEST PLAN

The silty sand soil for the experiment was sourced from between Nongong South Road Station and Dongfeng South Road Station, part of Zhengzhou Rail Transit Line 1's first phase, at a depth of 9 meters shown in Figure 4. Once extracted, the soil sample was promptly sealed with wax and labeled to indicate its top and bottom. However, during the transportation process, the soil samples were greatly disturbed, and the physical property indicators in the natural state were difficult to control. Therefore, all the silt soil used in the test was reshaped silt soil. The soil retrieved from the construction site was dried and crushed in the laboratory and passed through a 2 mm sieve as shown in Figure 4. The basic property indicators of silty sand soil obtained through basic physical tests are shown in Table 2.

At present, there are various methods for preparing hollow cylindrical specimens. For sandy soil, there are sand drop method, water vibration method and wet compaction method. For clay, sometimes a thin-walled pipe cutting method is used to obtain undisturbed clay. The material selected in this article is silty soil, so the sand drop method is used to fill the sample layer by layer during the sample preparation process as represented in Figure 5.

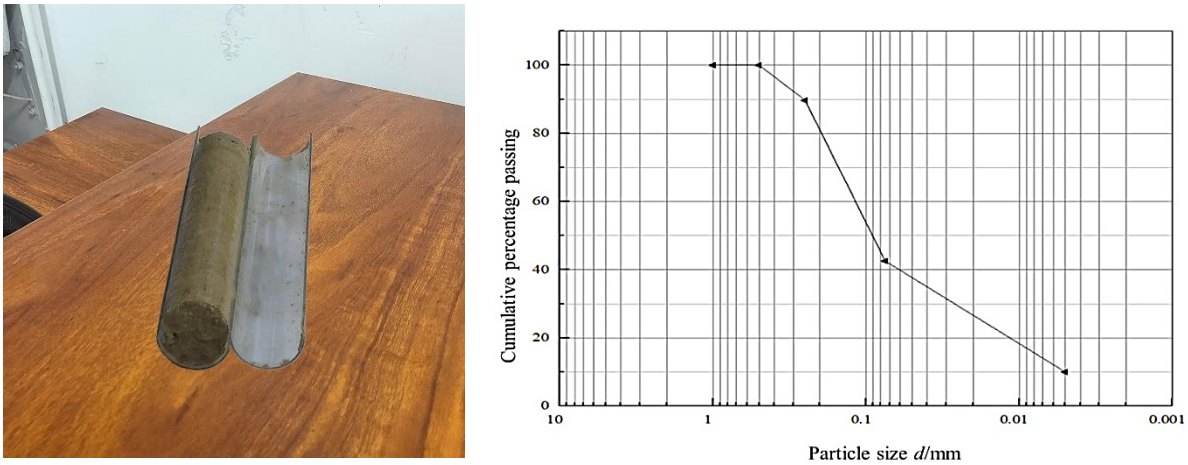

a) Undisturbed soil sample. (b) Gradation curve.

Fig. 4 a) Undisturbed soil sample, b) Particle grading curve of silty soil.

Table 2 Index properties of tested soil.

Specific gravity G_s	Moisture content w/%	Density ρ/ $(g.cm^{-3})$	Maximum void ratio e_{max}	Minimum void ratio e_{min}	Coefficient of uniformity C_u	Curvature coefficient C_c
2.63	23.54	1.64	0.93	0.51	4.43	1.19

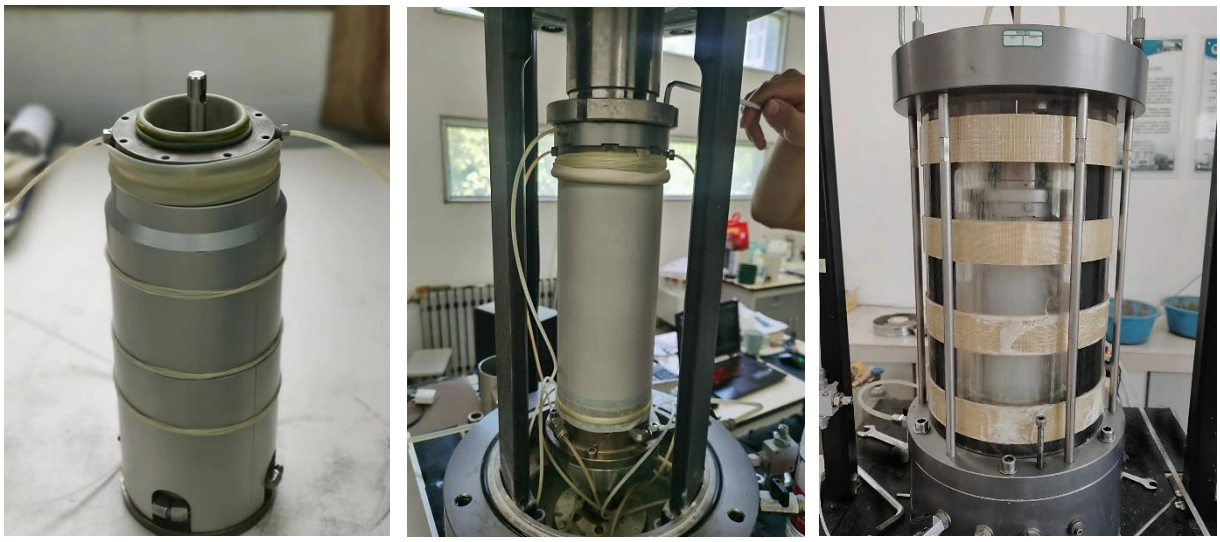

a) Install the top cover b) Install sample on the instrument c) Install pressure chamber cover

Fig. 5 Hollow cylinder sampling process; a) Install the top cover, b) Install sample on the instrument, c) Install pressure chamber cover.

Prepare the sample components by cleaning and wiping them with water, while inspecting the molds and pipelines in the pressure chamber to prevent pipeline blockage caused by silt. Ensure the outer rubber mold is leak-free using visual, air blowing, or water filling inspections. Assemble the inner membrane with a metal snap ring and O-ring for sealing, applying petroleum gel to the base card slot to prevent damage. Petroleum gel is known for its lubricating properties. When it can be added, it reduces friction between soil particles, making it nonstick with the side walls (Krishanthan, 2018). Insert the permeable stone and tighten it. Place filter paper on the permeable stone and cover the outer membrane on the base outer wall. Secure the outer three petal molds with rubber bands or fixtures. Create a 200 mm x 50 mm x 30 mm sample space. These dimensions were selected so as to minimize stress non-uniformities and ensure a middle height zone that remains unaffected by the boundary conditions (Sayao and Vaid, 1991) They also suggested a satisfactory geometry of the hollow cylinder specimen with regard to non-uniformity, and experimental control would be obtained if r_i/r_o were within 0.65 to 0.82. The present study has $r_i/r_o = 0.8$. To reduce the influence of radial friction, the height was recommended as

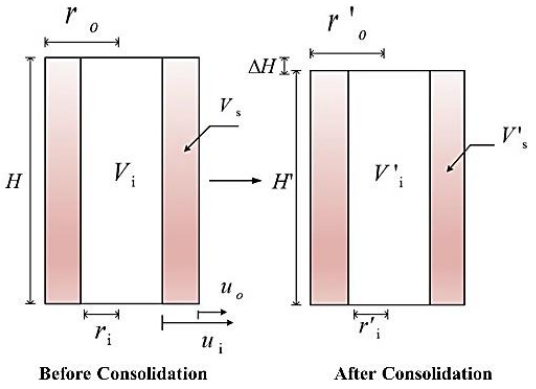

Fig. 6 Dimensional changes of hollow cylindrical specimens before and after consolidation.

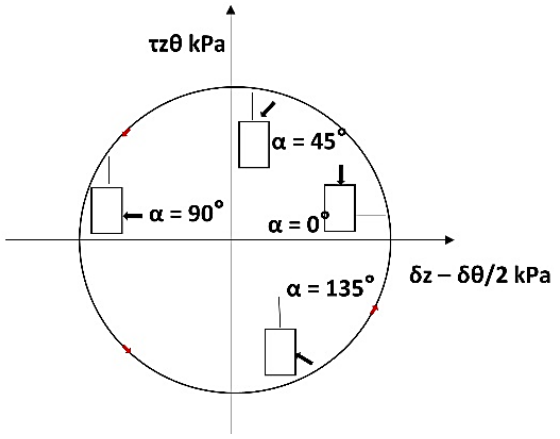

Fig. 7 Stress path under pure principal stress rotation.

$H/2r_o$ = 1.8– 2.2. Ongoing study employs $H/2r_o$ = 200/100 mm = 2. The aspect height to radius ratio is 2:1, chosen according to prior studies (Gräbe and Clayton, 2009; Guo et al., 2013).

First, weigh dried silty soil of 5 Kg approximately accordingly, then pour it into the mold in ten layers with a funnel and a spoon. In this process, keep the falling head at zero and use a rubber mallet to tap the mold to adjust the density of the specimen layer by layer. Divide the soil sample into 10 equal parts to pour evenly between the outer and inner layers, compact each layer to achieve the relative density of 50 ±2 hollow cylindrical shape of the sample achieved (Chen et al., 2020). Tie the upper part of the inner membrane with a rubber band to prevent soil from blocking the pipeline. Add filter paper on top, install the upper permeable stone, and secure the membranes. Ensure airtightness by applying negative pressure. Connect pore pressure and back pressure pipelines for airtightness inspection. Inject airless water into the sample's inner cavity. After removing the mold, fill with water, install the top cap and place the sample on the pressure chamber base. Control the GDSLAB to close the axis. Finally, seal the pressure chamber, apply 30 kPa pressure to the inner and outer confining pressures, and complete the sample production. Due to the compression of water pressure during the saturation and consolidation process of the sample, r_o and r_i get changed as shown in Figure 6, and the installation of measuring radius equipment is difficult. Therefore, the acquisition of ro and ri is calculated based on the changes in internal and external confining pressure, back pressure, and vertical displacement. After the change r_o'. The calculation formula for r_i' is as follows (Saada, 1988):

$$r_o' = \sqrt{\frac{r_o^2 H}{H'} - \frac{\Delta V_S + \Delta V_i}{\pi H'}} = \sqrt{\frac{r_o^2 H}{H - \Delta H} - \frac{\Delta V_S + \Delta V_i}{\pi (H - \Delta H)}} \quad (1)$$

$$r_i' = \sqrt{\frac{r_i^2 H}{H'} - \frac{\Delta V_i}{\pi H'}} = \sqrt{\frac{r_i^2 H}{H - \Delta H} - \frac{\Delta V_i}{\pi (H - \Delta H)}} \quad (2)$$

While, ΔV_s represents the volume change of the sample, and the drainage is positive, ΔV_i is the volume change in the inner cavity of the sample and the drainage is positive.

The description of the experimental setup is detailed in Table 3. The test parameters were followed according to prior studies (Wang et al., 2018b). This study primarily aims to assess how the coefficient of intermediate principal stress and the angle of principal stress rotation influence the stress-strain characteristics and pore pressure of silt soil during continuous principal stress axis rotation. To ensure homogeneity in the depth of the test samples, all samples were initially subjected to isotropic consolidation, where an effective average principal stress of 150 kPa was applied. Subsequently, the specimens underwent isotropic consolidation in accordance with the predetermined testing protocol. Following the completion of consolidation under drainage conditions, the average effective principal stress was consistently maintained at 150 kPa, while the deviator stress q was incrementally increased. Subsequently, the coefficient of intermediate principal stress was modified to achieve the desired value, leading to an 1800° rotation of the principal stress axis. The water drainage system in this experimental setup significantly influences the reduction of strain fluctuations during principal stress rotation (PSR), reduces the accumulation of pore water pressure, which can otherwise lead to increased plastic strains and potential liquefaction, and maintaining constant stress magnitudes while allowing for effective drainage results in lower strain fluctuations compared to undrained conditions (Wang et al., 2019). Based on the experimental setup, illustrate the relationship between the stress path and the principal stress axis's rotational angle in the τzθ – (δz – δθ)/2 graph, where δz represents the vertical normal stress and δθ the horizontal normal stress, as depicted in Figure 7.

Figure 8 illustrates the variation of internal and external confining pressures during the shear process of series C and ranging from 0 to 1. When the value of b is 0, the external pressure variation exceeds that of internal confining pressure. Conversely, when the value of b is 1, the variation of internal confining

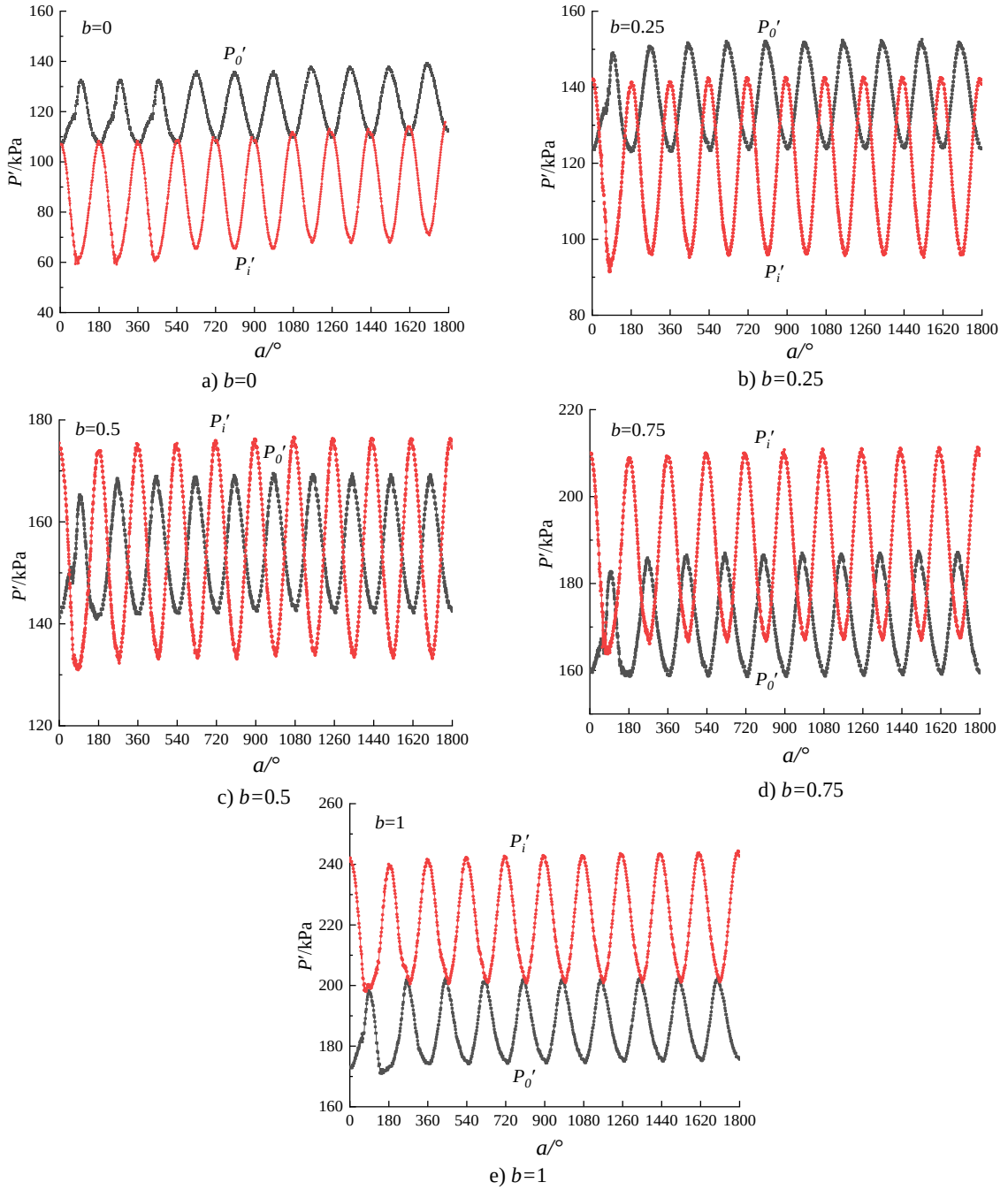

Fig. 8 Changes in internal and external confining pressure during shear proces a) b = 0, b) b= 0.25, c) b = 0.5, d) b = 0.75, e) b =1.

pressure surpasses that of the external pressure. Figure 9 shows the variation of axial force and torque during the shear process for series C, with axial force ranging from -0.6 kN to 0.6 kN and torque ranging from -15 kN to 15 kN.

3. RESULTS AND DISCUSSION

3.1. STRAIN DEVELOPMENT PATTERN IN DIFFERENT b VALUES

When the initial consolidation angle set to 0°, our investigation focused on comprehending the strain patterns associated with the rotation of principal stresses in various directions under different values of b. Figures 10 to 14 illustrated the results of the group C tests conducted on silt soil, emphasizing axial strain ε_z, radial strain ε_r, circumferential strain ε_θ and torsional shear strain $\gamma_{z\theta}$ .These figures demonstrated the development patterns, which depict that the strain behaviors of silt soil in different directions are impacted by the varying principal stress coefficients b.

Significantly, during the first rotation cycle (0° ~ 180°), the magnitude of strain fluctuations was more pronounced in all directions. However, as the principal stress axis continues to rotate, the magnitudes gradually diminish and eventually stabilize. This trend contrasts with Wang's

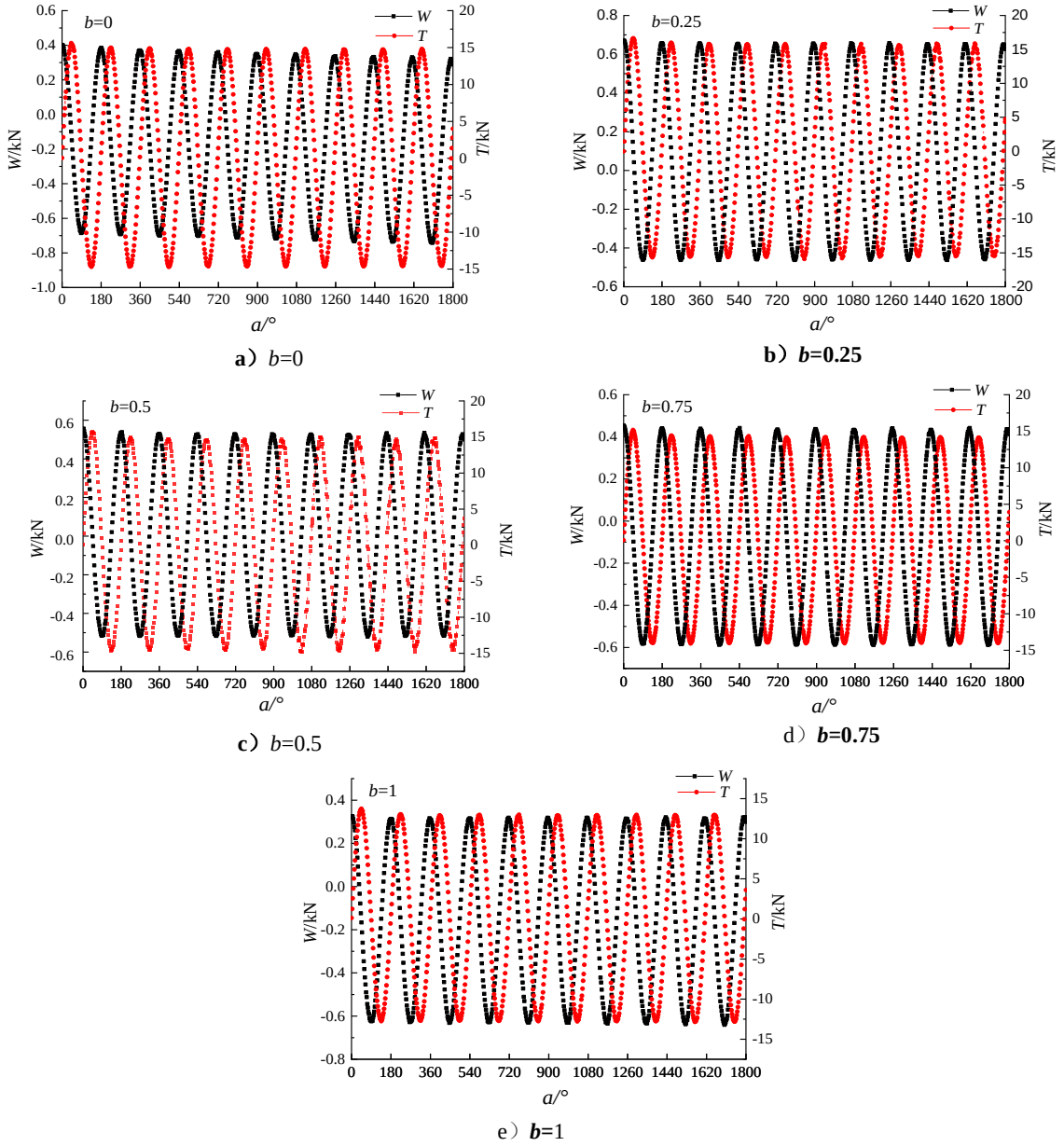

Fig. 9 Changes in axial force and torque during shearing process a) b = 0, b) b = 0.25, c) b = 0.5, d) b = 0.75, (e) b = 1.

Table 3 Hollow Cylinder test parameters.

Serial Number		Initial consolidation inclination angle ζ°	Coefficient intermediate principal stress b	Deviatoric stress q/*kPa*	Effective mean principal stress p'/*kPa*	Rotation range a°	Shear rate°/min
Series C	C101	0	0	140	150	Angle after consolidation-1800 degree	8
	C102		0.25				
	C103		0.5				
	C104		0.75				
	C105		1				

observations in Wenzhou soft clay (Wang et al., 2018b), where axial strain consistently increases with the continuous rotation of the stress principal axis. Therefore, it is crucial to comprehend that this divergence arises from a combination of various factors, including dissimilarities in the structural arrangement of the soil itself. Furthermore, Wang's experiments were conducted under undrained conditions where the continuous rotation of the stress principal axis along with the accumulation of pore pressure resulted in soil liquefaction and increased strain. In this research study, different experiments

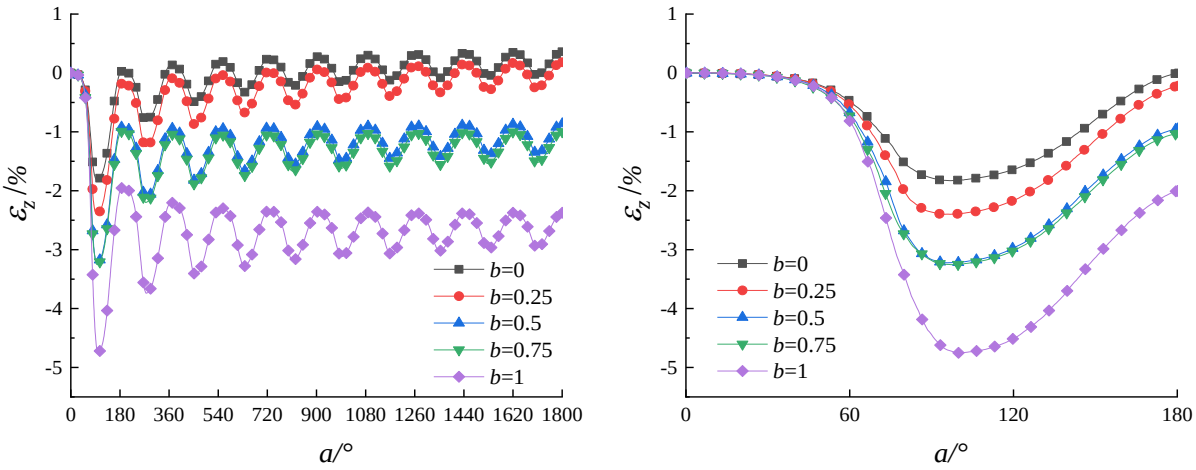

a) a= 0°~1800° b) a= 0°~180°

Fig. 10 Illustrate the pattern of axial strain development for various values of b a) a= 0°~1800°, b) a= 0°~180°.

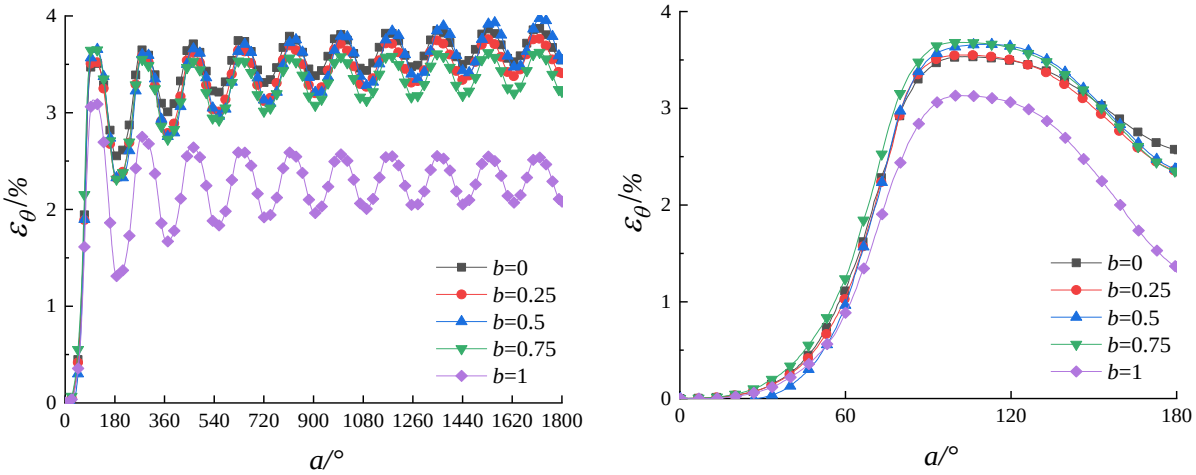

a) a= 0°~1800° b) a= 0°~180°

Fig. 11 Circumferential strain growth pattern under different values of b a) a= 0°~1800°, b) a= 0°~180.

were conducted under drainage conditions, with analysis of volumetric deformation reveals, that after substantial water drainage in the first rotation cycle the sample undergoes shear shrinkage followed by strain stabilization as the soil becomes more compact.

*3.1.1. AXIAL STRAIN DEVELOPMENT PATTERN IN DIFFERENT **b** VALUES*

Figure 10 depicts the progression of axial strain in relation to the rotation period under various b values. In the initial rotation period (0°~180°), the axial tensile strain experiences an initial increase, followed by a decrease, exhibiting a similar behavior to that observed by Wang's in Wenzhou soft clay, respectively (Wang et al., 2018b). While the rotation of the stress principal axis persists, the magnitude of axial strain fluctuations significantly stabilizes in the fourth rotation period (540°~ 720°). The stabilization of axial tensile strain during principal stress rotation is influenced by various factors, including the b value, which dictates the directionality and stabilization of strain, particularly for higher b values, suggesting a more uniform response across directions (Georgiannou et al., 2018).

Figures 10 to 14 further show, that the b value exerts a significant influence on the axial tensile strain, particularly at $b = 1$. As the b value decreases the magnitude of axial tensile strain diminishes. At b = 1, the soil demonstrates optimal tensile strain capacity, supporting greater tensile responses (Zhou et al., 2013). Whereas at $b = 0.25$ and $b = 0$, the axial strain gradually transits from axial tensile strain to axial compressive strain as it continuously rotates with the stress principal axis (Arthur et al., 1979). In the continuous rotation test of the stress principal axis, the pattern of axial strain development is less anisotropic between $b = 0$ and 0.25. However, the development curve of axial strain between $b = 0.5$ and 0.75, it almost coincides as the stress principal axis continuously rotates (Hicher and Lade, 1987; Higo, 2004).

The above results highlight that the sensitivity of axial strain in silty soil changes the intermediate principal stress coefficient b and the orientation of the

stress principal axis. It is also observed that larger b values enhance the alignment of soil particles with the major principal stress, leading to a more pronounced axial tensile strain. In contrast, the lower b values results, in a less ordered particle arrangement, potentially contributing to the transition from tensile to compressive strain. Continuous rotation of principal stress directions significantly affects soil behavior, with higher b values leading to rapid degradation and increased pore pressures (Hicher and Lade, 1987). The shear stiffness of soils decreases more rapidly with higher b values, indicating a shift in strain response under varying stress conditions (Zhou et al., 2013). This research contributes to the knowledge of the mechanical behavior of silty soils under varying stress conditions and provides valuable insights for engineering applications. Understanding of the strain behaviour aids in predicting soil deformation, which is vital for designing stable foundations (Kulhawy, 2004). Considering non-coaxial behavior and anisotropy in geotechnical engineering to ensure safety and stability has the potential to improve soil modeling and design methodologies (Tripura and Singh, 2016).

3.1.2. CIRCUMFERENTIAL STRAIN DEVELOPMENT PATTERN IN DIFFERENT VALUES OF b

The growth pattern of circumferential strain in relation to the rotation period, varying with different b values as shown in Figure 11. During the initial rotation period (0° ~ 180°), there is an increase followed by a decrease in circumferential compressive strain. It is worth noting that when $b = 1$, the circumferential compressive strain reaches its lowest point (Wang et al., 2018b). As the principal stress axis continues to rotate, the curve of circumferential compressive strain remains relatively stable within the range of 2-2.5 %. The lowest circumferential compressive strain observed when b = 1 signifies a critical point in the stress response of silty soil, where stress redistribution occurs most effectively, resulting in minimal deformation. This suggests that at b = 1, the soil achieves a balanced state that allows it to accommodate stress without significant compressive strain. In contrast, other b values lead to higher circumferential compressive strains, indicating less efficient stress management and potentially greater deformation during rotation. This comparison highlights the impact of b values on the soil's mechanical behavior, with b = 1 promoting stability and lower strain accumulation during stress rotation. The development curves of circumferential compressive strain for other b values significantly overlap. As the principal stress continues to rotate, the circumferential compressive strain values in the tenth rotation cycle range from 3-4 %, showing a gradual increase (Gutierrez et al., 2009). The observed phenomenon of circumferential compressive strain can be attributed to the plasticity of silty soil and the redistribution of stress during rotation. Silty soils commonly display plastic behavior, manifesting deformation under stress. The rotation of the principal stress axis leads to a redistribution of stress in the soil within the specimen. With continued rotation of the principal axis, the sample reaches a state where it achieves equilibrium between stress redistribution and deformation. The equilibrium state observed in silty soil during principal stress rotation, where stress redistribution occurs without significant deformation, is influenced by several interrelated mechanisms. Firstly, the plasticity of silty soils allows them to deform under stress without considerable volume change, enabling adaptation to new stress states while maintaining stability (Houlsby, 1981). Additionally, as the principal stress axis rotates, the soil particles rearrange, resulting in a redistribution of stress within the soil matrix, which helps balance internal forces and minimizes localized stresses that could lead to excessive deformation (Gutierrez et al., 2009). The shear resistance of silty soils contributes positively to stability, it is essential to recognize that factors such as soil composition and loading rates can also lead to reduced shear strength, particularly in saturated conditions (Najjar et al., 2007; Zhang et al., 2018).

The key differences in circumferential strain behaviour between the first rotation cycle and later cycles lie primarily in the initial increase and subsequent stabilization of strain. During the first rotation cycle (0° to 180°), circumferential compressive strain shows a notable increase, followed by a decrease, reflecting the soil's initial response to stress redistribution. This initial fluctuation is more pronounced due to the soil's adjustment to the changing stress conditions (Kim et al., 1992). In contrast, as the principal stress axis continues to rotate in later cycles, circumferential compressive strain values tend to stabilize, remaining relatively consistent within a narrower range (e.g., 2 % to 2.5 %) after the initial adjustments. This stabilization indicates that the soil has reached a more equilibrium state, where further rotations lead to less significant changes in strain, reflecting improved stress distribution and compactness as the cycles progress (Joer et al., 1998; Wichtmann et al., 2004). While, the first cycle exhibits dynamic behaviour, subsequent cycles show a trend toward consistency and stability in circumferential strain responses. The results of the present study are concurrent with the previous studies (Wang et al., 2018b; Gutierrez et al., 2009) and provide the significant knowledge to understand the behavior of silty soil.

3.1.3. RADIAL STRAIN DEVELOPMENT PATTERN IN DIFFERENT VALUES OF b

In Figure 12, the analysis reveals distinct patterns in the dispersion of radial strain relative to the rotation period across different b values, indicating significant anisotropy. During the first cycle, radial tensile strain is evident when $b = 0$, while samples with varying b values exhibit radial compressive strain. Notably, as the b value increases, the magnitude of radial strain also increases. However, the amplitude of radial strain

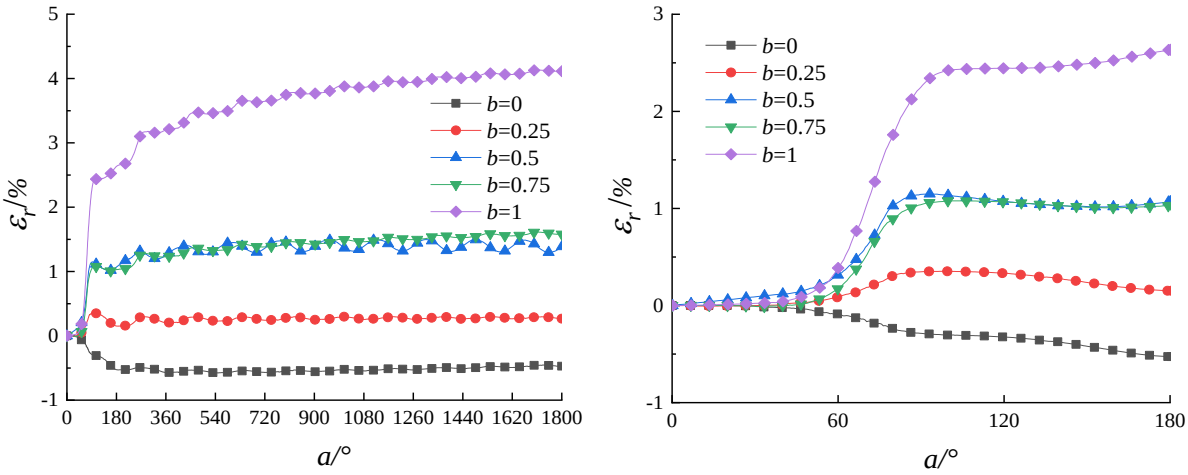

Fig. 12 Radial strain growth pattern under different values of b values a) a= 0°~1800°, b) a= 0°~180.

fluctuates and diminishes with successive cycles. In the tenth cycle, radial compressive strain for $b = 1$ continues to rise while for other b values, it remains relatively steady. The development curves of radial strain for $b = 0.5$ and 0.75 closely align with the continuous rotation of the principal stress axis and shows a lesser degree of anisotropy compared to axial strain.

The observed differences in radial strain behavior at various b values can be attributed to the influence of principal stress directions. Specifically, when $b = 0$, the soil experiences radial tensile strain during the initial cycle. This phenomenon arises due to the alignment of the principal stress direction, which results in an initial expansion in the radial direction. The decreasing amplitude of radial strain fluctuations with each subsequent cycle suggests the progressive deformation of the soil. As the principal stress axis continues to rotate, the soil particles undergo reorganization and adapt to changing stress conditions. This finding revels that the magnitude of radial strain fluctuations diminishes with each successive cycle, suggesting a gradual deformation of the silty soil. Results well agreed with the previous study. (Zhang et al., 2020; Zhou et al., 2014, 2013). This understanding can guide engineers in evaluating soil stability under dynamic loading conditions and better predict strain development in earth structures.

*3.1.4. TORSIONAL SHEAR STRAIN DEVELOPMENT PATTERN IN DIFFERENT VALUES OF **b***

As illustrated in Figure13, the concentration of torsional shear strain in relation to the rotation period is most prominently manifested under diverse b values, thereby denoting minimal anisotropic characteristics. Among all the strains, the torsional shear strain exhibits the most diminutive magnitude. Initially, in the first cycle, torsional shear strain experiences an upward trend followed by a subsequent decline. In the sixth cycle of rotation (900°~1080°), the magnitude of axial strain fluctuations in the silt soil tends to stabilize. While in the tenth rotation cycle, the torsional shear strain values encompass a range of - 0.2 - 0.7 % (Wang et al., 2023).

In the examination of the pure rotation test for principal stress, it is clearly noticeable that the trends in the curve of each strain component remain fundamentally the same across different values of b. The manifestation of anisotropy becomes evident in each strain component during the initial cycle commencing at approximately 60° of rotation. It is worth noting that among the various strain components, the magnitude of b has the most profound influence on the anisotropy of radial strain, while it has the least impact on torsional shear strain. The anisotropic attributes of each stress component are most prominent when $b = 1$ as compared to other values of b. Additionally, the development curves of the four stress components with $b = 0.5$ and 0.75 almost coincide with the rotation period. At b=1, the stress interactions reach a threshold, where the material's inherent properties and the loading conditions align, leading to noticeable anisotropic behavior earlier in the rotation at 60°. Conversely, other b values might result in a more uniform distribution of stress, delaying the emergence of anisotropy until 90° (Shen et al., 2024).

In our analysis of the deformation characteristics of fully saturated silty soil under different b values, we measure strain by evaluating the proportion of the variation in specimen volume during experimental loading to the initial volume of the specimen after consolidation has been accomplished. The equation 3 employed for this computation can be expressed as follows:

$$\varepsilon_v = \frac{\Delta V}{V_c} \tag{3}$$

To enable stress-strain analysis in the experiment, we have established a consistent convention. In the event that the specimen is in a drained state during the process of shearing, an augmentation in volume alteration ($\Delta V > 0$) corresponds to positive volumetric strain ($\varepsilon_v > 0$),

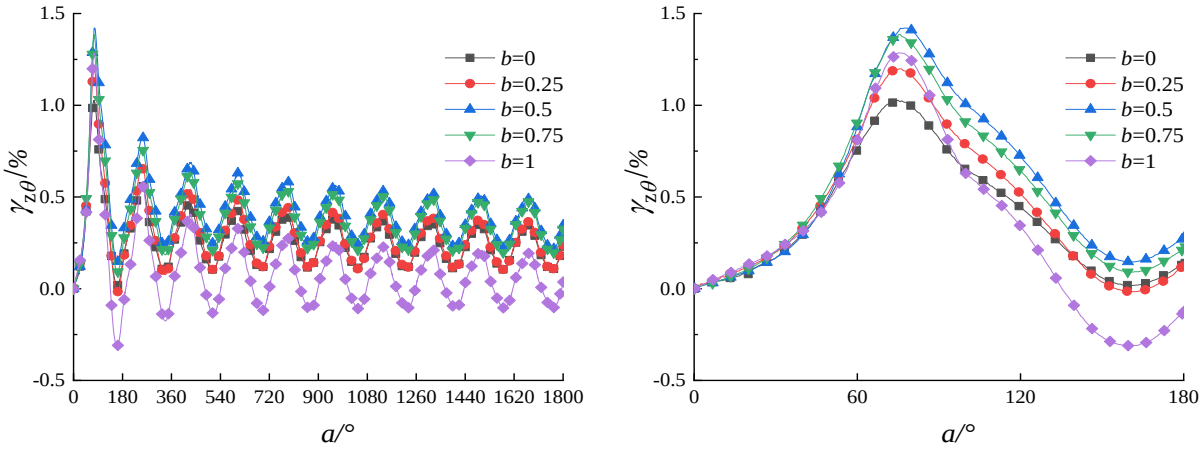

a) a= 0°~1800° b) a= 0°~180°

Fig. 13 Torsional shear strain increment pattern under different values of b: a) a= 0°~1800°, b) a= 0°~180°.

indicating contraction of the specimen during loading. Conversely, if the specimen is in a state of absorbing water and there is a reduction in volume alteration (ΔV <0), it produces negative volumetric strain (ε_v < 0), signifying expansion of the specimen during loading.

In summary, as the shear stress escalates, the volumetric strain also increases, leading to a decrease in specimen volume, showing a phenomenon of shrinkage. Conversely, when the shear stress intensifies and ε_v diminishes, the specimen volume increases, indicating a phenomenon of dilation. When the shear stress decreases and the specimen volume diminishes, it is referred to as unloaded volume shrinkage. On the other hand, when the shear stress decreases and the specimen volume increases, it signifies unloaded volume expansion.

The relationship between shear stress magnitude and volumetric strain in soil can be explained by the compaction and rearrangement of soil particles. When shear stress increases, it causes the soil to become more compacted, resulting in a decrease in specimen volume (shrinkage). On the other hand, when shear stress decreases, it allows the soil particles to rearrange and expand, leading to an increase in specimen volume (dilation). This behaviour aligns with the principles of soil mechanics and can be attributed to changes in inter-particle forces and void space during shearing. This study suggests that the minimal magnitude of silty soil to torsional shear strain is influenced by the arrangement of particles and their ability to maintain stability when subjected to rotations of principal stress (Wang et al., 2023). These findings have practical implications for geotechnical engineering applications. By understanding how soil deformation patterns change under different stress conditions, including shear stress magnitude and stress axis rotation, engineers can enhance the design and analysis of foundations, embankments, and other geotechnical structures. This knowledge can be utilized to predict and mitigate potential issues related to ground movement and deformation (Ding et al., 2023; Wang et al., 2023).

*3.1.5. VOLUMETRIC STRAIN DEVELOPMENT PATTERN IN DIFFERENT **b** VALUES*

Observing Figure 14, it becomes evident that when the volumetric strain ε_v surpasses 0, the sample finds itself in a drained state, leading to a decrease in volume and subsequent shrinkage. This phenomenon bears resemblance to the results of Xue Long's stress axis rotation test, where shrinkage was likewise observed. The relationship between volumetric strain and the rotation of the principal stress axis remains consistent under the influence of different b values. Initially, the rate of volumetric strain exhibits a linear increase during the first two cycles (0°~360°), but subsequently decelerates after reaching 360°. Results are similar to previous studies (Fredlund and Pham, 2006). It is worth noting that the sample possessing a b value of 1 commences to manifest anisotropy at approximately a rotation of 60°, while the remaining samples initiate to display anisotropy at around a rotation of 90° (Wan and Guo, 2001). Additionally, in the initial two cycles, the sample with a b value of 1 undergoes the least amount of shrinkage, while the sample with a b value of 0.5 experiences the most substantial shrinkage (Gebhardt et al., 2010). By the tenth cycle, the sample with a b value of 0 encounters the least amount of shrinkage, whereas the sample with a b value of 0.5 exhibits the most notable shrinkage (Chertkov, 2005).

The observation of the variation in volumetric strain in relation to the rotation of the principal stress axis at different b values is a significant finding. The results indicate that the rate of volumetric strain increases linearly during the initial two cycles (0°~360°) and then slows down after reaching 360°. This pattern suggests that the silty soil experiences substantial volume changes early in the stress rotation process, which then stabilize as the stress axis continues to rotate. This study made a significant contribution in the understanding of drained silty soil that the deformation response is strongly influenced by the direction of loading and b value. This study highlights the complex deformation behavior of soil

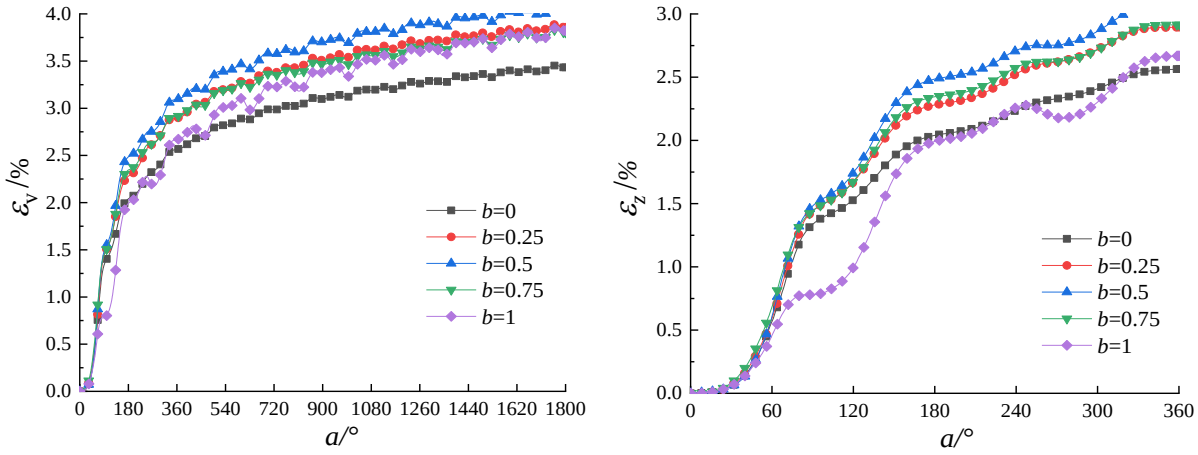

a) a= 0°~1800° b) a= 0°~360°

Fig. 14 Volumetric strain increment pattern under different values of b a) a = 1800^0, b) a = 360^0.

under cyclic stress rotation, emphasizing the importance of considering factors such as anisotropy, and stress conditions in geotechnical analyses.

3.2. PATTERN OF SHEAR STRESS-STRAIN DEVELOPMENT AT DIFFERENT b VALUES

Figure 15 (a) to (e) portrays the progression patterns of shear stress and strain for series C in the experimentation of the rotation of the principal stress axis. These examinations were executed by maintaining a constant principal stress coefficient throughout a range of cyclic cycles. In order to enhance the process of observation, we have opted to utilize the curves from the 1st, 3rd, 5th, 7th, and 10th cycles as exemplar instances from different b values for our comprehensive analysis.

Figure 15 (a) to (e) illustrates that different principal stress conditions result in noticeable hysteresis characteristics in the curve of the shear stress-strain relationship. While the shape of the shear stress-strain hysteresis loop is similar across different specimen variations in shear stiffness. During the initial and second cycles, all specimens exhibit unclosed hysteresis loops, which signify high plastic deformation and low shear stiffness, indicating the soil's inability to recover from stresses (Bocheńska and Srokosz, 2024). In the first cycle, representing exceptionally large double amplitude shear strain values. As the cycle duration increases, the hysteresis loops gradually shift from unclosed to closed forms in the 3rd and 5th cycle, this shift signifies a reduction in plastic deformation and an increase in shear stiffness, indicating that the soil is adapting to the stress conditions and becoming more resilient (Martins et al., 2024). The stress-strain curve exhibits a noticeable alteration in the shape of the hysteresis loop as a consequence of the rotation of the principal stress axis. In 7th and 10th hysteresis loops progressively decrease in size after each cycle, resulting in a decrease in the amplitude of shear strain and an increase in the values of shear strain reduction that are positive. Smaller loops demonstrate stabilization and reduced strain fluctuations, reflecting the soil's adaptation (Huang et al., 2024). Ultimately, this leads to an improvement in the rigidity of shear and eventually achieving stabilization. These modifications are ascribed to the significant impact of the rotation of the principal stress axis on the composition of silty soil, resulting in the development of a relatively stable soil structure that experiences less plastic deformation over time.

The behaviour of silty soil is influenced by various principal stress conditions, with a particular focus on the principal stress coefficient b. The soil's response is greatly affected by the value of b, resulting in variations in its behavior. These changes in stress conditions produce unique hysteresis patterns between shear stress and strain. The present study highlighted the importance of the rotation of the principal stress axis in shaping the composition and structure of silty soil, which in turn affects the characteristics of the hysteresis loop and the development of a relatively stable soil structure with reduced plastic deformation over time, which depicted the significance of the ongoing research. The hysteresis loop behavior in shear stress-strain relationships shows the soil's plastic deformation and subsequent stabilization, offering insights into shear strength and stiffness evolution, which is critical for designing structures under cyclic or rotating stress conditions (Bocheńska and Srokosz, 2024; Le et al., 2024).

Examining Figure 16 a), it becomes apparent that during the first cycle shear strain achieves its maximum at b=0.5 and diminishes as the b value deviates further from 0.5, either converging towards 0 or 1. The ultimate plastic strain arises during the first cycle, and by the conclusion of the third cycle, the hysteresis loop is closed. The shear modulus of the specimen is affected by radial restrictions, and as the rotation duration elongates, the specimen progressively stabilizes, culminating in a reduction of the hysteresis loop.

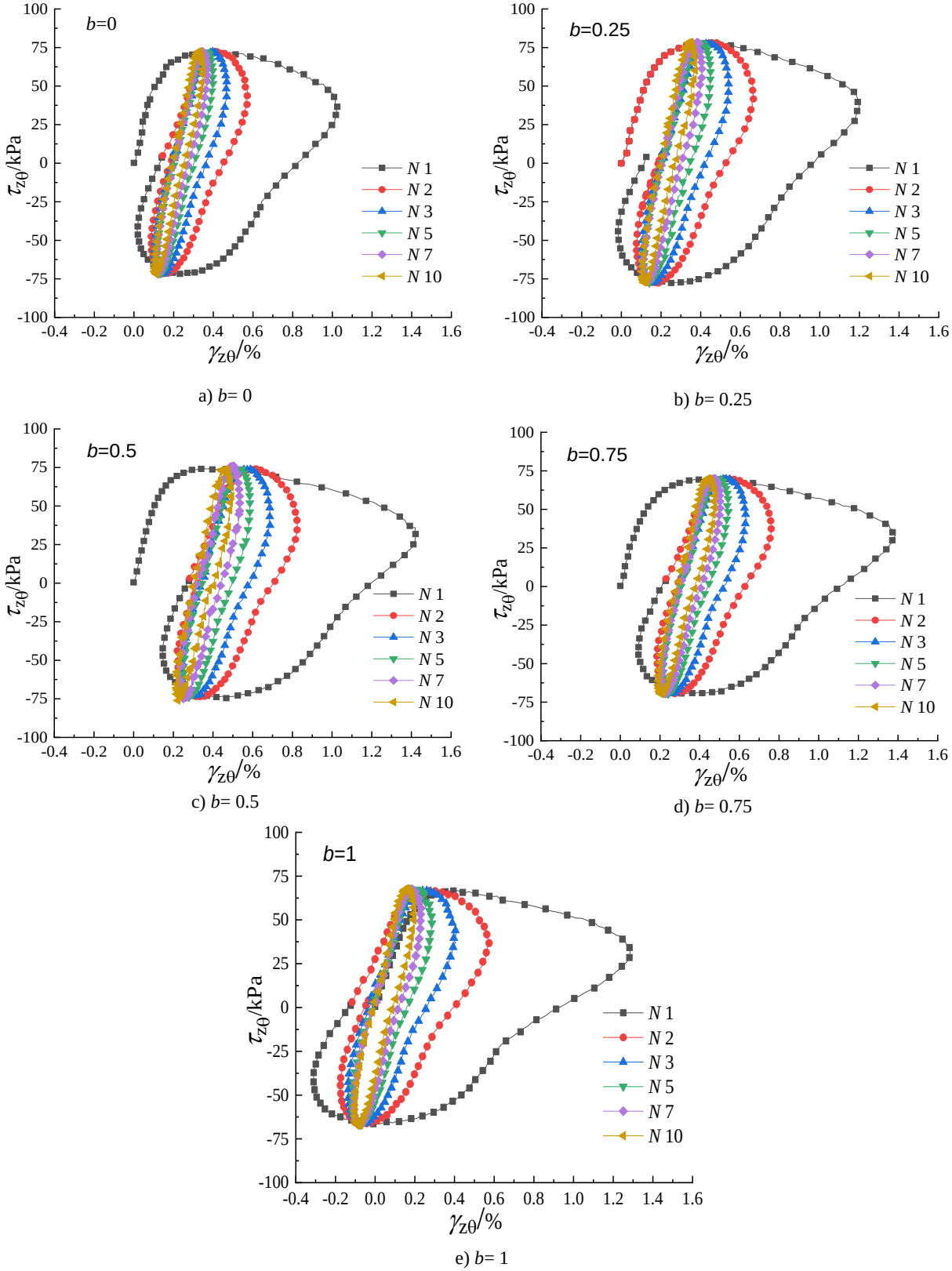

a) b= 0

b) b= 0.25

c) b= 0.5

d) b= 0.75

e) b= 1

Fig. 15 Pattern of shear stress-shear strain at distinct number of cycles and fixed b values a) b = 0, b) b = 0.25, c) b = 0.5, d) b = 0.75, e) b = 1.

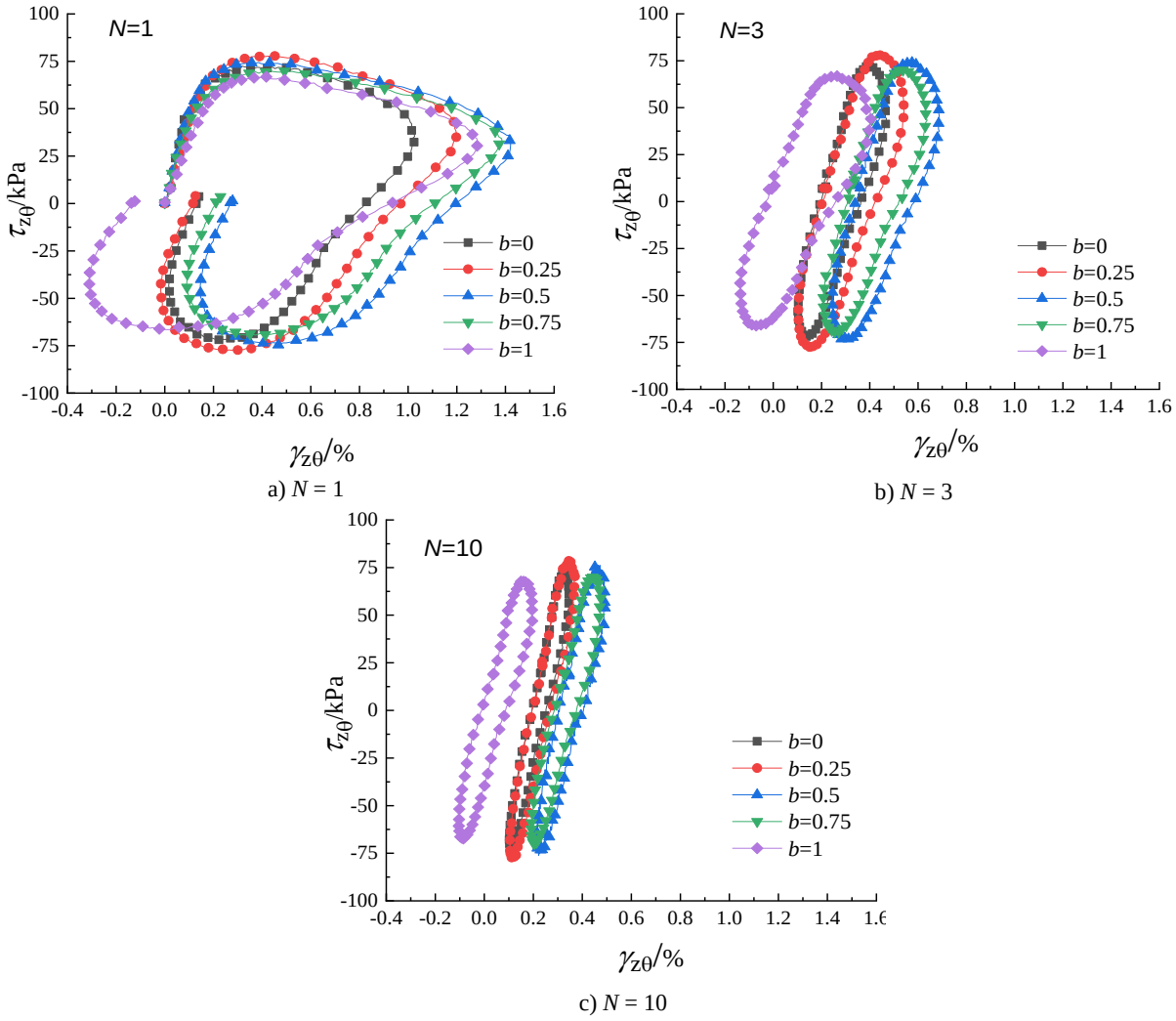

Fig. 16 Pattern of shear stress-shear strain development at distinct *b* values a) *N* = 1, b) *N* =3, c) *N* = 10.

The results highlighted that the initial cycle demonstrates the highest values of shear strain, indicating the occurrence of plastic deformation. This cycle is characterized by significant irreversible deformation of the silty soil contributing to the formation of a hysteresis loop. The accumulation of plastic strain significantly influences the open hysteresis loops in shear stress-strain curves by reflecting the soil's inability to fully recover from applied stresses. In the silty soil, when the soil experiences repeated loading, plastic deformation occurs, leading to unclosed hysteresis loops that indicate energy dissipation and a limited ability to elastic recovery (Bocheńska and Srokosz, 2024). This behavior is particularly pronounced in the initial cycles of loading, where the soil structure is still adjusting to the stress conditions. As the test progresses, the extent of plastic deformation decreases, resulting in a more closed hysteresis loop. The specimen gradually stabilizes, as the duration of rotation increases which can be attributed to adjustments in the microstructure of the soil. Over time, the silty soil particles may reorganize and compact, leading to an enhancement in the shear modulus and a reduction in plastic deformation. The shear modulus is influenced by radial restrictions such as confining stresses and boundary conditions. The interaction between shear and radial stresses plays a role in the changes observed in the behaviour of the specimen. The presence of radial restrictions and constraints leads to a more closed hysteresis loop, indicating soil stabilization. The transition from high shear strain in the first cycle to reduced shear strain in subsequent cycles suggests the presence of viscoelastic behavior. Initially, the soil exhibits a more viscous response with significant plastic deformation. However, as time progresses, the soil behaves in a more elastic manner, resulting in a decrease in the magnitude of shear strain. The value of b affects the anisotropy and shear stiffness of the silty soil. When *b*=0.5 the sample displays characteristics that lead to the maximum shear strain in the first cycle. Deviating from *b*=0.5 causes variations in soil behavior, producing shear strain to converge towards either extreme, depending on the specific value of *b*. The observation is in good accordance with the experiment

conducted on sand (Tong et al., 2010; Yang et al., 2007) and clay (Qian et al., 2018; Zhou et al., 2013). The principal stress coefficient b value, significantly influences soil behavior under stress, particularly in terms of tensile and compressive responses. Higher b values typically enhance tensile responses, leading to increased plastic strain during deformation (Mukuhira et al., 2024). While lower b values induce compressive behavior, leading to tighter hysteresis loops as the soil structure stabilizes more rapidly (Li and Xie, 2023). The initial direction of the major principal stress can dictate how disruptions interact, further modifying the hysteresis loop shape and energy dissipation characteristics (Takahashi et al., 2000).

3.3. NON-COAXIAL BEHAVIOR OF SILTY SOIL

Numerous laboratory tests indicate that geo-materials consistently show non-coaxiality, which is defined by the misalignment between the principal stress direction and the principal strain increment direction. Many researchers have focused on the non-coaxial behavior of soil and found that it has a significant effect on geotechnical engineering analysis and design. Neglecting the influences of non-coaxiality in geotechnical design may lead to potential hazards.(Gutierrez et al., 1991; Yang and Yu, 2006; Qian et al., 2008; Wang et al., 2018a). It is difficult to differentiate between the elastic strain increment and the total strain increment. Gutierrez et al. (1991) conducted studies which suggest that the elastic strain increment can be ignored due to its significantly smaller contribution to the total strain increment compared to the plastic strain increment. Instead of focusing on the plastic strain increment, the analysis of non-coaxiality utilizes the total strain increment. The angle β represents non-coaxiality and is defined as the angle between the principal stress direction α and the principal strain increment direction βdε. Non-coaxility calculated by using the equation (Wang et al., 2019).

$$\beta = \beta d\varepsilon - \alpha \tag{4}$$

$$\beta d\varepsilon = \frac{1}{2}\, tan^{-1} \frac{d\gamma z\theta}{d\varepsilon z - d\varepsilon\theta} \tag{5}$$

Figure 17 illustrates the relationship between the degree of non-coaxiality (β) and the major principal stress direction (α) for a test series conducted at ζ°= 0° under various *b* values (*b* = 0, 0.25, 0.5, 0.75, 1). Focusing on the initial rotation period, as shown in Figure 17(a), it was observed that the β angle decreased as the principal stress direction (α) increased from 0° to 45°, followed by an increase in β as α continued from 45° to 90°. As the principal stress direction (α) shifted from 90° to 180°, the β angle initially decreased, reaching its minimum at α = 135°, before starting to rise again. During the pure principal stress rotation tests, the β angle varied between 18° and 42°. During the rotation of pure principal stress tests, the β angle encompassed a range of values spanning from 18° to 42°. The results trends were similar (Qian et al., 2018; Wang et al., 2018a). The third rotation illustrated in Figure 17(b) was had a consistent pattern as followed in the first rotation cycle. It can be inferred that the identical generational pattern manifested for various *b* values while, within the equivalent predominant principal stress orientation, the magnitude of the β angle diminished in correspondence with the escalating *b* values. The reduced non-coaxial behavior at higher *b* values indicates a more aligned response between the direction of principal stresses and the resultant strains in the soil. This alignment suggests that as *b* increases, the soil behaves in a more isotropic manner, minimizing the angular discrepancy (β) between the stress and strain directions (Gutierrez et al., 2009; Lintao, 2013). As the principal stress direction shifts, the soil's ability to accommodate deformation becomes more coordinated at higher *b* values, leading to less non-coaxiality (Zdravkovic and Jardine, 1997). This knowledge is essential for improving the accuracy of geotechnical models and predicting soil behavior in scenarios where stress orientations change, such as in deep foundations or slopes (Cai et al., 2013; Zhou et al., 2014).

4. VALIDATION OF EXPERIMENTAL STUDY

The validity of this study, which focuses on the strain behaviors of silty soil under rotating principal stress axes and varying principal stress coefficients *b*, can be demonstrated through several key aspects.

The results of this study are extensively compared with previous findings, particularly those from (Wang et al., 2018b) on Wenzhou soft clay, which provides a reliable benchmark. While this study reveals differences in strain behavior between silty soil and soft clay, the divergence is explained logically, considering factors such as differences in soil structure and experimental conditions (drained vs. undrained). For example, the increase in axial strain during the first rotation cycle aligns with Wang's findings, but the strain stabilization observed here in drained conditions provides a distinct contribution to the body of knowledge. This ability to contextualize and explain deviations from established research enhances the validity of the study.

The investigation encompasses axial, radial, circumferential, and torsional shear strains, offering a comprehensive analysis of soil behavior. The study identifies consistent trends across multiple strain components, such as the pronounced fluctuation in strain during the initial rotation cycles followed by stabilization which are consistent with known soil mechanics principles. The congruence of patterns across strain components and the use of multi-directional strain analysis reinforce the robustness of the findings.

By conducting tests for different values of the intermediate principal stress coefficient *b*, the study reveals the significant influence of this parameter on soil behavior. The variation in strain magnitudes for different *b* values (e.g., the maximum axial tensile

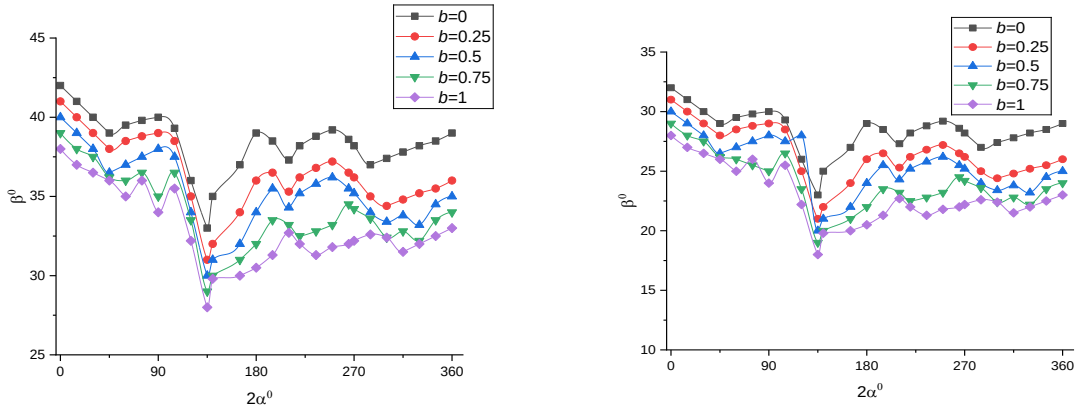

Fig. 17 The relationship between degrees of non-coaxiality and principal stress direction with ζ°= 0, a) *N*=1st cycle b) *N*=3rd cycle.

strain at b = 1 and the transition to compressive strain at lower b values) is consistent with known theories on the effects of intermediate principal stress. Additionally, the study's findings on the influence of b on the anisotropy of strain components are in good agreement with prior research, particularly (Zhou et al., 2013) and (Arthur et al., 1979), which strengthens the reliability of the results.

The observation of strain stabilization, particularly in the fourth rotation period for axial strain and later for other components, provides evidence of the soil's adjustment to the applied stress conditions. This trend aligns with established mechanical behavior in soils under cyclic loading, where deformation tends to stabilize as the soil structure adapts. The detailed discussion of anisotropic behavior, particularly in radial strain (notably for higher b values), is well-founded, supported by previous studies such as Hicher and Lade (1987) and Zhang et al. (2020). The consistent manifestation of anisotropy further corroborates the validity of the strain analysis.

The analysis of hysteresis loops in the shear stress-strain relationship across different cycles is critical for assessing soil behavior under cyclic loading. The study's finding that hysteresis loops become progressively more closed with each rotation cycle, indicating a reduction in plastic deformation, is a well-established phenomenon in soil mechanics. This observation is consistent with earlier studies (Bocheńska and Srokosz, 2024); (Martins et al., 2024) and adds credibility to the claim that soil stabilization occurs after several cycles of stress axis rotation. The agreement between the stress-strain behavior of silty soil in this study and prior research on sand (Tong et al., 2010; Yang et al., 2007) and clay (Qian et al., 2018; Zhou et al., 2013) further supports the validity of the experimental findings.

The study validates its findings on non-coaxiality by comparing the angle between the principal stress direction and the strain increment direction with previous research. The results, which show that the β angle decreases as b increases, agree with the established understanding of non-coaxial soil behavior (Gutierrez et al. 1991; Yang and Yu, 2006). The consistency in the β angle pattern across different b values, as shown in Figure 17, and the comparison with other studies on non-coaxiality in geo-materials (Qian et al., 2018; Wang et al., 2018a), further enhance the reliability of the data.

5. CONCLUSION

This study focus is to investigate how principal stress rotation affects silt soil, utilizing a hollow cylindrical apparatus. Thoroughly explored the influence of cycle count on the static characteristics of saturated silty soil, particularly focusing on the intermediate principal stress coefficient b and rotational angle a. The following conclusions are drawn;

1. The principal axis of stress continued to rotate the amplitude of strain fluctuation initially decreased and eventually reached a stable state. In the pure rotation test of principal stress, the overall trend observed in each strain component plot remained consistent regardless of the specific b value. However, during the first cycle, a certain degree of anisotropy became apparent in each strain component at around 60° of rotation. The influence of b values varied among the strain components, with radial strain being the most affected and torsional shear strain being the least affected.
2. The distinct principal stress conditions led to the emergence of unique hysteresis characteristics within the curve representing the relationship between shear stress and strain. Although the hysteresis loop for shear stress and strain appeared similar across different specimens, there were noticeable variations in shear stiffness. All specimens exhibited unclosed hysteresis loops for shear stress and strain during the initial and second cycles, with the first cycle showing significantly large double amplitude shear strain

values. With an increase in cycle duration the hysteresis loops transitioned from unclosed to closed forms.

3. The hysteresis loops observed in the shear stress-strain curves display variations depending on the b values and the initial direction of the major principal stress. These loops initially remain open, thereby denoting the accumulation of plastic strain. With an increase in the b values, there is a discernible deterioration in stiffness.
4. Stiffness degradation was observed during the rotation of pure principal stresses. The impact of b values and a angle on the deterioration of stiffness is significant. When the b values increase, the ratio of stiffness decreases.
5. Across various values of b, the volumetric strain exhibits an initial linear increase for two cycles before decelerating after 360°. It is noteworthy that at an angle of 60°, $b = 1$ demonstrates anisotropy, whereas the other values exhibit this phenomenon at 90°. In terms of overall shrinkage, $b = 0$ experiences the least amount of contraction after ten cycles, while $b = 0.5$ exhibits the most significant decrease in volume.
6. The intermediate principal stress coefficient b values exerted a notable impact on the non-coaxial behaviour of silty soil as the degrees of non-coaxial behaviour diminished with higher b-values. The alteration of non-coaxial behaviour in silty soil is contingent upon the initial orientation of the principal stress.
7. The research provides a comprehensive analysis of the anisotropic properties of saturated silt soil under drained conditions, considering factors such as stress relationships, deformation patterns, volumetric changes, and strength characteristics.
8. Future research should examine how loading rates, and drainage conditions affect silty soil non-coaxial behaviour and overall performance when subjected to stress rotation.

CREDIT AUTHORSHIP CONTRIBUTION STATEMENT

Farhad Jamil: Conceptualization, Methodology, Writing original draft, visualization. **Changnv Zeng:** Conceptualization, Writing – review & editing, Project administration, Supervision. **Yuan Ma:** Data curation and software. **Soe Hlaing Tun:** Review & editing, data curation. **Sharafat Ali:** Review & editing.

ACKNOWLEDGEMENT

This research is funded by Henan Province Joint Fund Project of Science and Technology (grant number 222103810075), the Innovative Funds Plan of Henan University of Technology (grant number 2022ZKCJ07).

REFERENCES

Arthur, J.R.F., Chua, K.S. and Dunstan, T.: 1979, Dense sand weakened by continuous principal stress direction rotation. Géotechnique, 29, 91–96. DOI: 10.1680/geot.1979.29.1.91

Bocheńska, M. and Srokosz, P.E.: 2024, Artificial neural network-aided mathematical model for predicting soil stress-strain hysteresis loop evolution. Civ. Environ. Eng. Rep., 34, 120–135. DOI: 10.59440/ceer/190839

Cai, Y., Yu, H.-S., Wanatowski, D. and Li, X.: 2013, Noncoaxial behavior of sand under various stress paths. J. Geotech. Geoenviron. Eng., 139, 1381–1395. DOI: 10.1061/(ASCE)GT.1943-5606.0000854

Chen, G., Wu, Q., Zhou, Z., Ma, W., Chen, W., Khoshnevisan, S. and Yang, J.: 2020, Undrained anisotropy and cyclic resistance of saturated silt subjected to various patterns of principal stress rotation. Géotechnique, 70, 317–331. DOI: 10.1680/jgeot.18.P.180

Chertkov, V.Y.: 2005, The shrinkage geometry factor of a soil layer. Soil Sci. Soc. Am. J., 69, 1671–1683. DOI: 10.2136/sssaj2004.0343

Cui, L., Sheng, Q., Niu, Z. and Chang, L.: 2021, Deformation behavior of saturated sarine silt under principal stress rotation as induced by wave loading. Appl. Sci., 11, 9458. DOI:10.3390/app11209458

Dareeju, B., Gallage, C., Ishikawa, T. and Dhanasekar, M.: 2017, Effects of principal stress axis rotation on cyclic deformation characteristics of rail track subgrade materials. Soils Found., 57, 423–438. DOI: 10.1016/j.sandf.2017.05.009

Ding, Z., Chen, Y., He, S.-H. and Sun, M.-M.: 2023, Investigating the long-term deformation behaviour and non-coaxiality of siliceous sand under traffic cyclic loading. Constr. Build. Mater., 408, 133672. DOI: 10.1016/j.conbuildmat.2023.133672

Fredlund, D.G. and Pham, H.Q.: 2006, A volume-mass constitutive model for unsaturated soils in terms of two independent stress state variables. In: Unsaturated Soils 2006. Presented at the Fourth International Conference on Unsaturated Soils, American Society of Civil Engineers, Carefree, Arizona, United States, 105–134. DOI: 10.1061/40802(189)4

Gallage, C., Dareeju, B., Dhanasekar, M. and Ishikawa, T.: 2016, Effects of principal stress axis rotation on unsaturated rail track foundation deterioration. Procedia Eng., 143, 252–259. DOI: 10.1016/j.proeng.2016.06.032

Gao, Z. and Zhao, J.: 2017, A non-coaxial critical-state model for sand accounting for fabric anisotropy and fabric evolution. Int. J. Solids Struct., 106–107, 200–212. DOI: 10.1016/j.ijsolstr.2016.11.019

Gebhardt, S., Fleige, H. and Horn, R.: 2010, Shrinkage processes of a drained riparian peatland with subsidence morphology. J. Soils Sediments, 10, 484–493. DOI: 10.1007/s11368-009-0130-9

Georgiannou, V.N., Konstadinou, M. and Triantafyllos, P.: 2018, Sand behavior under stress states involving principal stress rotation. J. Geotech. Geoenviron. Eng., 144, 04018028. DOI: 10.1061/(ASCE)GT.1943-5606.0001878

Gräbe, P.J. and Clayton, C.R.: 2009, Effects of principal stress rotation on permanent deformation in rail track foundations. J. Geotech. Geoenviron. Eng., 135, 555–565. DOI: 10.1061/(ASCE)1090-0241(2009)135:4(555)

Guo, L., Fang, Y., Wu, T., Wang, J., Jin, H. and Shi, L.:2021, Cyclic behavior of sand under traffic loading with 'Inclined' consolidation. KSCE J Civ Eng, 25, 1621–1633. DOI: 10.1007/s12205-021-0892-1

Guo, L., Wang, J., Cai, Y., Liu, H., Gao, Y. and Sun, H.: 2013, Undrained deformation behavior of saturated soft clay under long-term cyclic loading. Soil Dynamics and Earthquake Engineering, 50, 28–37. DOI: 10.1016/j.soildyn.2013.01.029

Gutierrez, M., Ishihara, K. and Towhata, I.: 1991, Flow theory for sand during rotation of principal stress direction. Soils Found., 31, 121–132. DOI: 10.3208/sandf1972.31.4_121

Gutierrez, M., Wang, J. and Yoshimine, M.: 2009, Modeling of the simple shear deformation of sand: effects of principal stress rotation. Acta Geotech., 4, 193–201. DOI: 10.1007/s11440-009-0094-3

Hicher, P. and Lade, P.V.: 1987, Rotation of principal directions in K0-consolidated clay. J. Geotech. Eng., 113, 774–788. DOI: 10.1061/(ASCE)0733-9410(1987)113:7(774)

Hight, D.W., Gens, A. and Symes, M.J.: 1983, The development of a new hollow cylinder apparatus for investigating the effects of principal stress rotation in soils. Géotechnique, 33, 355–383. DOI: 10.1680/geot.1983.33.4.355

Higo, Y.: 2004, Instability and strain localization analysis of water-saturated clay by elasto-viscoplastic constitutive models, Kyoto University, (in Chinese). DOI: 10.14989/doctor.k10813

Houlsby, G.T.: 1981, Study of plasticity theories and their applicability to soils. Apollo-University of Cambridge Repository. DOI: 10.17863/CAM.14121

Huang, J., Sun, X., Li, X., Gao, Y., Chen, J., Fu, X. and Liu, S.: 2024, Deformation behaviors of saturated clay under intermittent cyclic loading with cyclic confining pressure. Int. J. Geomech., 24, 06024009. DOI: 10.1061/IJGNAI.GMENG-8927

Inam, A., Ishikawa, T. and Miura, S.: 2012, Effect of principal stress axis rotation on cyclic plastic deformation characteristics of unsaturated base course material. Soils Found., 52, 465–480. DOI: 10.1016/j.sandf.2012.05.006

Ishihara, K. and Towhata, I.: 1983, Sand response to cyclic rotation of principal stress directions as induced by wave loads. Soils Found., 23, 11–26. DOI: 10.3208/sandf1972.23.4_11

Jardine, R.J., Potts, D.M., Fourie, A.B. and Burland, J.B.: 1986, Studies of the influence of non-linear stress–strain characteristics in soil–structure interaction. Géotechnique, 36, 377–396. DOI: 10.1680/geot.1986.36.3.377

Joer, H.A., Lanier, J. and Fahey, M.: 1998, Deformation of granular materials due to rotation of principal axes. Géotechnique, 48, 605–619. DOI: 10.1680/geot.1998.48.5.605

Kim, D.-S., Stokoe II, K.H. and Hudson, W.R.: 1992, Deformational characteristics of soils at small to intermediate strains from cyclic tests. Interim Report.

Krishanthan, K.: 2018, Influence of principal stress rotation on the behaviour of soft railway subgrade (PhD). University of Wollongong, Australia.

Kulhawy, F.H.: 2004, On the axial behavior of drilled foundations. GeoSupport Conference 2004, American Society of Civil Engineers, Orlando, Florida, United States, 34–51. DOI: 10.1061/40713(2004)3

Kumruzzaman, M. and Yin, J.-H.: 2012, Influence of the intermediate principal stress on the stress–strain–strength behaviour of a completely decomposed granite soil. Géotechnique, 62, 275–280. DOI: 10.1680/geot.8.P.025

Lade, P.V. and Kirkgard, M.M.: 2000, Effects of stress rotation and changes of b-values on cross-anisotropic behavior of natural. Soils Found., 40, 93–105. DOI: 10.3208/sandf.40.6_93

Le, V.H., Glasenapp, R. and Rackwitz, F.: 2024, Cyclic hysteretic behavior and development of the secant shear modulus of sand under drained and undrained conditions. Int. J. Geomech., 24, 04024126. DOI: 10.1061/IJGNAI.GMENG-9380

Li, Q. and Xie, Z.: 2023, Analysis of spatiotemporal variations in *b*-values before the 6.8-magnitude earthquake in Luding, Sichuan, China, on September 5, 2022. Research Square, preprint. DOI: 10.21203/rs.3.rs-3102786/v1

Lintao, Y.: 2013, Experimental study of soil anisotropy using hollow cylinder testing. Ph.D thesis, University of Nottingham, United Kingdom.

Martins, L.A., Correia, A.A.S., Venda Oliveira, P.J. and Lemos, L.J.L.: 2024, Effect of the cyclic loading on the yield surface of a chemically stabilised soil. Proc. Inst. Civ. Eng. Ground Improv., 177, 392–400. DOI: 10.1680/jgrim.24.00036

Miura, K., Miura, S. and Toki, S.: 1986, Deformation behavior of anisotropic dense sand under principal stress axes rotation. Nak. Soils Found., 26, 36–52. DOI: 10.3208/sandf1972.26.36

Mukuhira, Y., Fehler, M.C., Bjarkason, E.K., Ito, T. and Asanuma, H.: 2024, On the *b*-value dependency of injection-induced seismicity on geomechanical parameters. Int. J. Rock Mech. Min. Sci., 174, 105631. DOI: 10.1016/j.ijrmms.2023.105631

Najjar, S.S., Gilbert, R.B., Liedtke, E., McCarron, B. and Young, A.G.: 2007, Residual shear strength for interfaces between pipelines and clays at low effective normal stresses. J. Geotech. Geoenviron. Eng., 133, 695–706. DOI: 10.1061/(ASCE)1090-0241(2007)133:6(695)

Nakata, Y., Hyodo, M., Murata, H. and Yasufuku, N.: 1998, Flow deformation of sands subjected to principal stress rotation. Soils Found., 38, 115–128. DOI: 10.3208/sandf.38.2_115

Qian, J.-G., Du, Z.-B. and Yin, Z.-Y.: 2018, Cyclic degradation and non-coaxiality of soft clay subjected to pure rotation of principal stress directions. Acta Geotech., 13, 943–959. DOI: 10.1007/s11440-017-0567-8

Qian, J.G., Yang, J. and Huang, M.S.: 2008, Three-dimensional noncoaxial plasticity modeling of shear band formation in geomaterials. J. Eng. Mech., 134, 322–329. DOI: 10.1061/(ASCE)0733-9399(2008)134:4(322)

Saada, A.: 1988, State-of-the-Art Paper: Hollow cylinder torsional devices: Their advantages and limitations. In: Proc. Advanced Triaxial Testing of Soil and Rock, Donaghe, R. and Silver, M. (Eds.). ASTM International, 766–789. DOI: 10.1520/STP29113S

Sayao, A. and Vaid, Y.P.: 1991, A critical assessment of stress nonuniformities in hollow cylinder test specimens. Soils Found., 31, 60–72. DOI: 10.3208/sandf1972.31.60

Shamoto, Y., Zhang, J.-M. and Tokimatsu, K.: 1998a, New charts for predicting large residual post-liquefaction ground deformation. Soil Dyn. Earthq. Eng., 17, 427–438. DOI: 10.1016/S0267-7261(98)00011-6

Shamoto, Y., Zhang, J.-M. and Tokimatsu, K.: 1998b, Methods for evaluating residual post-liquefaction ground settlement and horizontal displacement. Soils Found., 38, 69–83. DOI: 10.3208/sandf.38.Special_69

Shen, P., Wang, Q., Fang, J., Wang, C. and Zhang, K.: 2024, Analysis of strength characteristics of loess before and after freezing using a hollow cylinder torsional shear apparatus. Res. Cold Arid Reg., 16, 63–72. DOI: 10.1016/j.rcar.2024.04.003

Symes, M.J., Gens, A. and Hight, D.W.: 1988, Drained principal stress rotation in saturated sand. Géotechnique, 38, 59–81. DOI: 10.1680/geot.1988.38.1.59

Symes, M.J.P.R., Gens, A. and Hight, D.W.: 1984, Undrained anisotropy and principal stress rotation in saturated sand. Géotechnique, 34, 11–27. DOI: 10.1680/geot.1984.34.1.11

Takahashi, S., Echigoya, J. and Motoki, Z.: 2000, Magnetization curves of plastically deformed Fe metals and alloys. J. Appl. Phys., 87, 805–813. DOI: 10.1063/1.371945

Tong, Z.-X., Zhang, J.-M., Yu, Y.-L. and Zhang, G.: 2010, Drained deformation behavior of anisotropic sands during cyclic rotation of principal stress axes. J. Geotech. Geoenviron. Eng., 136, 1509–1518. DOI: 10.1061/(ASCE)GT.1943-5606.0000378

Wichtmann, T., Niemunis, A. and Triantafyllidis, T.: 2004, The effect of volumetric and out-of-phase cyclic loading on strain accumulation. Conference: Cyclic behaviour of soils and liquefaction phenomena. Taylor & Francis. DOI: 10.1201/9781439833452.ch31

Tripura, D.D.and Singh, K.D.: 2016, Behavior of cement-stabilized rammed earth circular column under axial loading. Mater Struct, 49, 371–382. DOI: 10.1617/s11527-014-0503-4

Wan, R.G. and Guo, J.: 2001, Drained cyclic behavior of sand with fabric dependence. J. Eng. Mech., 127, 1106–1116. DOI: 10.1061/(ASCE)0733-9399(2001)127:11(1106)

Wang, J., Feng, D., Guo, L., Fu, H., Cai, Y., Wu, T. and Shi, L.: 2019, Anisotropic and noncoaxial behavior of K0-consolidated soft clays under stress paths with principal stress rotation. J. Geotech. Geoenviron. Eng., 145, 04019036. DOI: 10.1061/(ASCE)GT.1943-5606.0002103

Wang, S., Zhong, Z., Chen, B., Wu, B., Zhang, D. and Ni, F.: 2023, Experimental study on strain accumulation characteristics of saturated remolded loess under pure rotation of the principal stress axis. Front. Ecol. Evol., 11, 1275648. DOI: 10.3389/fevo.2023.1275648

Wang, Y., Gao, Y., Cai, Y.and Guo, L.: 2018a, Effect of initial state and intermediate principal stress on noncoaxiality of soft clay–involved cyclic principal stress rotation. Int. J. Geomech., 18, 04018081. DOI: 10.1061/(ASCE)GM.1943-5622.0001214

Wang, Y., Gao, Y., Guo, L., Cai, Y., Li, B., Qiu, Y. and Mahfouz, A.H.: 2017. Cyclic response of natural soft marine clay under principal stress rotation as induced by wave loads. Ocean Eng., 129, 191–202. DOI: 10.1016/j.oceaneng.2016.11.031

Wang, Y., Gao, Y., Guo, L.and Yang, Z.: 2018b, Influence of intermediate principal stress and principal stress direction on drained behavior of natural soft clay. Int. J. Geomech., 18, 04017128. DOI: 10.1061/(ASCE)GM.1943-5622.0001042

Wang, Y., Gao, Y., Li, B., Guo, L., Cai, Y. and Mahfouz, A.H.: 2019, Influence of initial state and intermediate principal stress on undrained behavior of soft clay during pure principal stress rotation. Acta Geotech., 14, 1379–1401. DOI: 10.1007/s11440-018-0735-5

Wang, Z., Liu, P., Jeng, D.and Yang, Q.: 2017, Cyclic strength of sand under a nonstandard elliptical rotation stress path induced by wave loading. J. Hydrodyn., 29, 89–95. DOI: 10.1016/S1001-6058(16)60720-5

Wang, Z., Yang, Y., Li, Y., Liu, S. and Zhou, P.: 2022, Numerical simulation of cyclic shear tests considering the fabric change and principal stress rotation effects. Int. J. Numer. Anal. Methods Geomech., 46, 1409–1432. DOI: 10.1002/nag.3351

Wang, Z., Yang, Y., Lu, N., Li, Y. and Yu, H.-S.: 2019, Effects of the principal stress rotation in numerical simulations of geotechnical laboratory cyclic tests. Comput. Geotech., 109, 220–228. DOI: 10.1016/j.compgeo.2019.01.023

Wong, R.K.S. and Arthur, J.R.F.: 1986, Sand sheared by stresses with cyclic variations in direction. Géotechnique, 36, 215–226. DOI: 10.1680/geot.1986.36.2.215

Yang, Y. and Yu, H.S.: 2006, A non-coaxial critical state soil model and its application to simple shear simulations. Int. J. Numer. Anal. Meth. Geomech., 30, 1369–1390. DOI: 10.1002/nag.531

Yang, Z.X., Li, X.S. and Yang, J.: 2007, Undrained anisotropy and rotational shear in granular soil. Géotechnique, 57, 371–384. DOI: 10.1680/geot.2007.57.4.371

Yoshimine, M., Ishihara, K. and Vargas, W.: 1998, Effects of principal stress direction and intermediate principal stress on undrained shear behavior of sand. Soils Found., 38, 179–188. DOI: 10.3208/sandf.38.3_179

Zdravkovic, L. and Jardine, R.J.: 1997, Some anisotropic stiffness characteristics of a silt under general stress conditions. Géotechnique, 47, 407–437. DOI: 10.1680/geot.1997.47.3.407

Zhang, F., Chen, G.X., Wu, Q. and Zhou, Z.-L.: 2019, Experimental study on undrained behavior of saturated silt subject to wave loading. Rock Soil Mech., 40, 2695–2702. DOI: 10.16285/j.rsm.2018.0410

Zhang, S.-G., Chen, L. and Liu, W.-B.: 2020, Experimental study on strain characteristics and non-coaxilty of saturated silty clay under principal stress axis rotation. J. Highw. Transp. Res. Dev., 37. DOI: 10.3969/j.issn.1002-0268.2020.06.002

Zhang, T., Cai, G. and Liu, S.: 2018, Reclaimed lignin-stabilized silty soil: Undrained shear strength, Atterberg limits, and microstructure characteristics. J. Mater. Civ. Eng., 30, 04018277. DOI: 10.1061/(ASCE)MT.1943-5533.0002492

Zhou, J., Yan, J., Liu, Z. and Gong, X.: 2014, Undrained anisotropy and non-coaxial behavior of clayey soil under principal stress rotation. J. Zheijang Univ.-Sci., 15, 241–254. DOI: 10.1631/jzus.A1300277

Zhou, J., Yan, J., Xu, C. and Gong, X.: 2013, Influence of intermediate principal stress on undrained behavior of intact clay under pure principal stress rotation. Math. Probl. Eng., 2013, 1–10. DOI: 10.1155/2013/950143

Zhou, R., Zhang, F. and Zhao, K.: 2018, Experimental study on excess pore pressure and deformation of saturated silt under complex stress paths. J. Nat. Disasters, 27, 173–179.